Astronomy & Astrophysics manuscript no. SED_paper_s1
October 28, 2018

The impact of stars stripped in binaries on the integrated spectra of stellar populations

Y. Götberg[1], S. E. de Mink[1,2], J. H. Groh[3], C. Leitherer[4], and C. Norman[5]

[1] Anton Pannekoek Institute for Astronomy, University of Amsterdam, 1090 GE Amsterdam, The Netherlands
e-mail: Y.L.L.Gotberg@uva.nl, S.E.deMink@uva.nl
[2] GRAPPA, GRavitation and AstroParticle Physics Amsterdam, University of Amsterdam, 1090 GE Amsterdam, The Netherlands
[3] School of Physics, Trinity College Dublin, The University of Dublin, Dublin 2, Ireland
[4] Space Telescope Science Institute, 3700 San Martin Drive, Baltimore, MD 21218, USA
[5] Dept. of Physics & Astronomy, Johns Hopkins University, Baltimore, MD 21218, USA

Received .....; accepted .....

ABSTRACT

Stars stripped of their envelopes by interaction with a binary companion emit a significant fraction of their radiation as ionizing photons. They are potentially important stellar sources of ionizing radiation, however, they are still often neglected in spectral synthesis simulations or simulations of stellar feedback. Anticipating the large datasets of galaxy spectra from the upcoming James Webb Space Telescope, we model the radiative contribution from stripped stars using detailed evolutionary and spectral models. We estimate their impact on the integrated spectra and specifically on the emission rates of H I-, He I-, and He II-ionizing photons from stellar populations.

We find that stripped stars have the largest impact on the ionizing spectrum of a population in which star-formation has halted several Myr ago. In such stellar populations, stripped stars dominate the emission of ionizing photons, mimicking a younger stellar population in which massive stars are still present. Our models also suggest that stripped stars have harder ionizing spectra than massive stars.

The additional ionizing radiation that stripped stars contribute with affects observable properties that are related to the emission of ionizing photons from stellar populations. In co-eval stellar populations, the ionizing radiation from stripped stars increases the ionization parameter (U) and the production efficiency of hydrogen ionizing photons ($\xi_{\rm ion,0}$). They also allow high values for these parameters for about ten times longer than what massive stars do. The effect on properties related to non-ionizing wavelengths is less pronounced, such as on the UV-continuum slope or stellar contribution to emission lines. However, the hard ionizing radiation from stripped stars likely introduce a characteristic ionization structure of the nebula, leading to emission of highly ionized elements such as O^{2+} and C^{3+}. We, therefore, expect that the presence of stripped stars affects the location in the BPT diagram and the diagnostic ratio of O III to O II nebular emission lines (O32). Our models are publicly available through CDS and as add-on to Starburst99.

1. Introduction

Spectra of stellar populations provide us with powerful tools to study stars and their host galaxies across cosmic time. Existing surveys and those anticipated with future facilities, such as James Webb Space Telescope (JWST, Gardner et al. 2006), are expected to deliver a wealth of observational data that can potentially revolutionize our understanding. Translating these data into measurements of the physical quantities of interest, such as star-formation rates, requires the use of theoretical or semi-empirical models for the spectra of stellar populations. Accurate models for the spectra of stellar populations and in particular the ionizing radiation are therefore indispensable (Conroy 2013).

Ionizing photons are of primary interest for two reasons. Ionizing photons from stellar sources can be reprocessed by nearby gas and dust, giving rise to infrared excess and various prominent emission lines (Charlot & Longhetti 2001). These include lines that are used as diagnostics to infer star-formation rates, metallicities, as well as possible variations in the initial stellar mass function and to infer the presence or absence of active galactic nuclei (AGN). The reliability of these measurements depends on the accuracy of the underlying models. Ionizing photons from stellar populations also play a crucial role as a source of stellar feedback. For example, it is thought to be important in regulating the efficiency of star-formation (Krumholz et al. 2006; Dale et al. 2013). On a larger scale, ionizing radiation from stellar populations that escapes the host galaxies can ionize gas in the intergalactic medium (IGM), which is generally held responsible for the reionization of the Universe (Barkana & Loeb 2001; Robertson et al. 2010; Lapi et al. 2017).

Traditionally, massive single stars have been considered to be the main producers of ionizing photons in stellar populations. They are rare and short-lived but have high luminosities of $\sim 10^4 - 10^6\,L_\odot$ and, with temperatures higher than $\sim 25\,000$ K, they emit most of their radiation at energies above the threshold for hydrogen ionization (e.g., Smith et al. 2002; Martins et al. 2005; Ekström et al. 2012; Köhler et al. 2015; Schneider et al. 2018). The most massive stars can eventually lose their hydrogen-rich envelopes as a result of strong stellar winds or eruptions creating Wolf-Rayet (WR) stars (Meynet & Maeder 2005), which can be so hot that they emit photons sufficiently energetic to ionize even helium (Crowther 2007).

Recent studies of nearby resolved stellar populations show that massive and intermediate mass stars are often accompanied by a companion star that orbits so close that interaction between the two stars is inevitable as the stars evolve and swell up (Sana et al. 2012; Moe & Di Stefano 2017). Interaction in binary systems can completely change the future evolution of the stars in the system, for example leading to mass accretion, rejuvenation, rapid rotation, mass loss, and possibly even coalescence (e.g., Vanbeveren et al. 1979; Podsiadlowski et al. 1992; Wellstein & Langer 1999; Eldridge et al. 2008; de Mink et al. 2014;

Schneider et al. 2015; Stanway & Eldridge 2018). Including, or improving the treatment of, the effects of binary interaction in models for the spectra of stellar populations is therefore warranted.

In this study, we focus on stars that have been stripped from their envelope as a result of interaction with a binary companion (Kippenhahn & Weigert 1967; Paczyński 1967). This is expected to be a very common outcome of binary interaction (e.g. Sana et al. 2012) resulting in very hot and compact stars (van der Linden 1987; Yoon et al. 2010, 2017). Because of their high temperatures, they are expected to emit the majority of their radiation at ionizing wavelengths (Götberg et al. 2017, hereafter Paper I). This makes them potentially important, but still often neglected, contributors to the budget of ionizing photons produced by stellar populations, as argued for example in Van Bever & Vanbeveren (2003) and Vanbeveren et al. (2007), see also Belkus et al. (2003) and Stanway et al. (2016).

One of the challenges to properly account for the impact of these stripped stars on the ionizing spectra of stellar populations, was, until recently, the scarcity of appropriate atmosphere models. Direct observations of stars stripped in binaries are still scarce, likely because they are typically outshone by their companion (see, however, Gies et al. 1998; Groh et al. 2008; Peters et al. 2008, 2013; Wang et al. 2017, 2018; Chojnowski et al. 2018). As a result, there had been very few requests for atmosphere models for stripped stars. The earliest estimates of the integrated spectra of stellar populations including stripped stars, therefore, relied on black-body approximations or rescaling of atmosphere models originally computed for more luminous WR stars. Modern simulations make use of spectral libraries, but these typically did not cover the full parameter space of interest for stripped stars or considered the effect of metallicity.

This motivated us to undertake the effort of computing an extensive library of evolutionary and spectral models custom-made for stripped stars that result from binary interaction for a range of masses and metallicities (Götberg et al. 2018, hereafter Paper II). In Paper I we showed how metallicity affects the stripping process. At lower metallicity, the progenitor star remains more compact leading to an incomplete stripping of the envelope. The resulting star is therefore partially stripped and more luminous but also cooler. In Paper II we presented large model grids that cover a range of masses and metallicities. We showed how these stars span a continuous range of spectral types, from WR-like spectra characterized by emission lines formed in the winds of the more massive and metal-rich stripped stars, to subdwarf-like spectra dominated by absorption features resulting from the photosphere of stripped stars with transparent outflows. We further predicted the existence of a hybrid intermediate class of spectra showing a combination of absorption and emission lines, very similar to those observed for the recently discovered new class of WN3/O3 stars (Massey et al. 2014, 2015, 2017; Neugent et al. 2017, 2018; Smith et al. 2018).

The aim of this work is to estimate the radiative contribution from stripped stars to the spectral energy distribution of stellar populations and measure the additional emission rate of ionizing photons that stripped stars produce. For this purpose, we developed a population synthesis code to estimate the number and type of stripped stars that are present in a population at any given time. We used the custom-made grid of spectral models for individual stripped stars that we published in Paper II. We use this to investigate the impact on the integrated spectra, We discuss the integrated spectra, the emission rate of H I-, He I-, and He II-ionizing photons, and further quantities that can be derived from observations, namely the production efficiency of ionizing photons, the ionization parameter, the UV luminosity and continuum slope, and stellar spectral features.

The first theoretical and semi-empirical studies of the integrated spectra of stellar populations primarily focussed on the effects of single stars. These include codes based on single star models, such as Starburst99 (Leitherer et al. 1999, 2010, 2014) GALAXEV (Bruzual & Charlot 2003), and PEGASE (Fioc & Rocca-Volmerange 1997, 1999; Le Borgne et al. 2004). However, more recently, several groups have considered the effects of binary interaction. These include the Brussels code (Van Bever et al. 1999; Belkus et al. 2003; Vanbeveren et al. 2007), the Yunnan simulations (Zhang et al. 2004; Han et al. 2010; Chen & Han 2010; Zhang et al. 2012; Li et al. 2012; Zhang et al. 2015), and the BPASS code (Eldridge & Stanway 2009, 2012; Eldridge et al. 2017). Starburst99 is a widely used code to model the spectra of young stellar populations. We will, therefore, use this to simulate and compare with the contributions of single stars. BPASS is an advanced and sophisticated code that accounts for various products of binary interaction. The authors have provided testable predictions for a large range of observable phenomena (Eldridge & Stanway 2012, 2016; Eldridge & Maund 2016; Eldridge et al. 2018; Stanway et al. 2014, 2016; Stanway & Eldridge 2018; Xiao et al. 2018). We will, therefore, compare our findings with BPASS predictions throughout this paper and discuss the similarities and differences we find.

Our hope is that the predictions provided in this work will be of use for the interpretation of the data that is resulting from several recent and ongoing surveys that are probing the ionizing properties of stellar populations. This includes the anticipated James Webb Space Telescope (Gardner et al. 2006), but our simulations are also interesting for various surveys currently conducted from the ground. For example, the MOSDEF survey (Kriek et al. 2015), the KBSS (Rudie et al. 2012; Steidel et al. 2014), the KLCS (Steidel et al. 2018), the GLASS (Treu et al. 2015), the VUDS (Le Fèvre et al. 2015), and the ZFIRE (Nanayakkara et al. 2016). We will, therefore, make our predictions available online in electronic format. They can be retrieved from the CDS database (INCLUDE LINK WHEN AVAILABLE) and they will also be available through the Starburst99 web-portal.

The structure of this paper is as follows. Section 2 briefly describes the models for the evolution and spectra of stripped stars that we presented previously in Paper II and how we use these to construct a model for the integrated spectrum of stripped stars in a stellar population. In Sect. 3, we show how the presence of stripped stars affects the total spectral energy distribution of a stellar population. We quantify the contribution from stripped stars to the emission rate ionizing photons in Sect. 4. In Sect. 5, we discuss the impact of stripped stars on observable quantities. In Sect. 6 we summarize our findings and conclusions. The current paper is the third in a series with Paper I and Paper II, but it can be read independently.

2. Accounting for the radiative emission from stripped stars in stellar populations

We create an estimate of the radiative contribution from the stripped stars in stellar populations. We first describe the models for the evolution of individual stripped stars and their spectra in Sect. 2.1. We then describe the assumptions that we make to model stellar populations in Sect. 2.2.

2.1. Models of individual stripped stars

Binary evolutionary models

We use the models presented in Paper II to describe the evolution of stars that lose their envelope through interaction with a binary companion (see also Paper I, for an in-depth discussion). These are models of binary systems in which stable mass transfer is initiated early during the Hertzsprung gap, after which the H-rich envelope is stripped off (commonly referred to as Case B type mass transfer, Kippenhahn & Weigert 1967). Stripped stars can also result from stable mass transfer initiated during the main-sequence evolution of the most massive star in the system (Case A type mass transfer, Kippenhahn & Weigert 1967), or from unstable mass transfer and a subsequent successful ejection of the common envelope (Paczynski 1976; Ivanova 2011). The contribution from the different formation channels vary depending on the progenitor mass, but we expect that Case B type mass transfer is responsible for the majority of the stripped stars. Despite the variety of evolutionary histories, the properties of the stripped stars are remarkably similar. These properties are primarily dependent on the mass of the stripped stars alone. This assumption works well for most systems, see however Claeys et al. (2011); Yoon et al. (2017); Siess & Lebreuilly (2018); Sravan et al. (2018) for evolution that leads to a larger fraction of the H-rich envelope is left, which is the case for systems with long initial periods or very low metallicity. We use our models of stripped stars created through Case B type stable mass transfer as an approximation for stripped stars formed via any evolutionary channel. This approximation is sufficient for our current purposes.

The evolutionary models were computed using the binary stellar evolution code MESA (Paxton et al. 2011, 2013, 2015, 2018). The models have the metallicities $Z = 0.014$, 0.006, 0.002, and 0.0002, which are representative of the metallicity of the Sun, the Large and Small Magellanic Clouds, and an environment with very low metallicity that may be representative of early stellar populations. Each metallicity grid consists of 23 models with different assumptions for the initial masses of the donor star, chosen between $M_{1,\,\mathrm{init}} = 2$ and $20\,M_\odot$ with equal spacing in the logarithm of the mass. All models were computed with a mass ratio of $q \equiv M_{2,\,\mathrm{init}}/M_{1,\,\mathrm{init}} = 0.8$ and mass transfer was initiated early during the Hertzsprung gap (applying initial periods between $P_{\mathrm{init}} = 3$ and 35 days). The resulting stripped stars have masses between 0.35 and $7.9\,M_\odot$. The wind mass-loss from stripped stars is an uncertain parameter because few stripped stars have been observed. The models, therefore, employ extrapolations of the wind mass-loss algorithm for hot and subluminous stars of Krtička et al. (2016) from the low mass end and of the empirical WR mass-loss recipe of Nugis & Lamers (2000) from the high mass end. The switch between the two wind regimes is chosen to occur for stripped stars with progenitor masses of $6\,M_\odot$. Low-mass stripped stars are affected by diffusion processes that impact the surface composition (Heber 2016). An algorithm accounting for the effect of gravitational settling (see Paxton et al. 2011, also Thoul et al. 1994 and Paquette et al. 1986) is included when modeling the evolution of stripped stars. It has strong effects for stripped stars with masses below $0.7\,M_\odot$ (see Paper II).

These large model grids cover the evolution of stripped stars from low to high mass. They stretch from stripped stars at the lower mass limit of central helium burning ($\sim 0.35\,M_\odot$, Han et al. 2002) and close to the mass limit where massive stars lose their envelope via their own wind (e.g., Chiosi & Maeder 1986). It is likely that stars of higher mass than what we consider experience envelope-stripping in binaries, for example, through mass-transfer initiated on the main sequence evolution of the donor star (see e.g., Yoon et al. 2010). However, these stars would primarily contribute at early stages because the progenitor stars are more massive and, therefore, live for a shorter time. Here, we focus on the contribution from stripped stars that can not have been created by strong wind mass-loss and, therefore, they have lower masses than most WR stars. For this mass range, we consider that our models are appropriate to use as a representation of the stellar evolution of stripped stars given the careful choices for the wind mass-loss rates and the treatment of diffusion processes on the stellar surfaces. We use the evolutionary models were as input for the spectral models described below. We also adopt the time of stripping and the duration of the stripped phase in our simulations of the integrated spectra of stellar populations, see Sect. 2.2.

Spectral models

The spectral models for individual stripped stars that we use in this work were computed with the non-LTE radiative transfer code CMFGEN (Hillier 1990; Hillier & Miller 1998) and were custom-made for stripped stars by employing the surface parameters given by the evolutionary models as input at the base of the atmosphere. The evolutionary models were used at the time when the stripped star had reached half-way through central helium burning ($X_{\mathrm{He,\,c}} = 0.5$). We can use these models as a good approximation for the spectral properties throughout most of the stripped star phases. This is because the luminosity and the effective temperature do not change significantly during most of the time the stars are stripped. The spectral models for individual stripped stars are publicly available at the CDS database[1].

The shape of the spectral energy distribution and the emission rates of ionizing photons (see Table 1 of Paper II) depend on the assumed wind mass-loss rates, wind speeds, and wind clumping. These parameters are uncertain. Theoretical predictions are now available (e.g., Krtička et al. 2016; Vink 2017), but they have not yet been thoroughly tested against observations, because only very few stripped stars with sufficiently strong wind mass-loss have been identified and studied in detail so far (e.g., Groh et al. 2008). In Paper I we showed that variations in wind mass-loss rate primarily affect the predicted emission rate of He II-ionizing photons, while the emission rates of H I- and He I-ionizing photons are not significantly affected. The mass-loss rates assumed in our models were chosen to smoothly connect the mass-loss rates of subdwarfs (Krtička et al. 2016) with the observed mass-loss rates of WR stars (Nugis & Lamers 2000). Our assumed mass-loss rates also match well with the observed mass-loss rate of the stripped star in the binary system HD 45166 (Groh et al. 2008). The recent theoretical predictions by Vink (2017) suggest that the mass-loss rates of stripped stars may be ten times lower than what we assume in this paper. The winds of stripped stars are likely not reaching close to the Eddington limit, in contrary to massive main-sequence and WR stars (cf. Bestenlehner et al. 2014). This suggests that the wind mass-loss rate from stripped stars is lower than that from WR stars and thus not well-described by the recipe for WR stars of Nugis & Lamers (2000). To establish which are the wind mass-loss rates from stripped stars, observations of a sample of stripped stars are necessary. If, as suggested by Vink (2017), the mass-loss

[1] http://vizier.cfa.harvard.edu/viz-bin/VizieR?-source=J/A+A/615/A78

rates from stripped stars indeed are lower than what the recipe from Nugis & Lamers (2000) predicts, it would imply an increase of the emission rates of He II-ionizing photons presented in this work. The emission rates of H I- and He I-ionizing photons are robust against wind uncertainties.

The wind parameters also affect the stellar spectral features. Higher wind mass-loss rate, slower winds, or stronger clumping result in stronger emission features as the stellar wind becomes denser. The wind speed could be slower than our assumptions. We assume terminal wind speeds of 1.5 times the escape speed of the surface of the stripped star, which results in values of $\sim 1500 - 2500$ km s^{-1}. The observed stripped star HD 45166 has an anisotropic wind that partially is slow, which gives rise to the strong emission lines the star exhibits (Groh et al. 2008). For a better understanding of the spectral features from stripped stars, an observed sample is necessary.

2.2. Modeling the contribution of stripped stars to a stellar population

We model the number and type of stripped stars that are present in a population as a function of time by taking a Monte Carlo approach. We first create a sample of stars by randomly drawing initial masses, $M_{\rm init}$, from the initial mass function of Kroupa (2001), $dN/dM_{\rm init} \propto M_{\rm init}^{\alpha}$, where $\alpha = -1.3$ for $M_{\rm init} < 0.5\,M_{\odot}$ and -2.3 for $M_{\rm init} > 0.5\,M_{\odot}$. We assume mass limits of $0.1\,M_{\odot}$ and $100\,M_{\odot}$. We then choose which stars that will have a companion star using the mass-dependent binary fraction of Moe & Di Stefano (2017) that follows closely the linear function $f_{\rm bin} = 0.09 + 0.63\log_{10}(M_{\rm init}/\,M_{\odot})$ (see also van Haaften et al. 2013). The mass of the companion stars are randomly drawn, such that the mass ratio, $q = M_{2,\,\rm init}/M_{1,\,\rm init}$, follows a flat distribution sampled between 0.1 and 1 (consistent with the observations of Kiminki & Kobulnicky 2012, Sana et al. 2012, and Moe & Di Stefano 2017, for early-type stars). The initial orbital periods are randomly drawn from a distribution that is flat in the logarithm of the period (e.g., Öpik 1924; Kouwenhoven et al. 2007; Moe & Di Stefano 2017). For systems where the most massive star of the system has a mass $M_{1,\,\rm init} \geq 15\,M_{\odot}$, we use the distribution by Sana et al. (2012), which favors short-period systems. As a lower limit for the initial period, we choose the shortest period that allows both stars to fit inside their Roche-lobes at zero-age main-sequence. For the upper limit of the initial period, we follow Moe & Di Stefano (2017) and set $10^{3.7}$ days.

We use evolutionary models of single stars to follow the radius evolution of the donor star and to determine when it will start to interact with its companion star. We created these models with MESA, using the same physical assumptions as we adopted for the models of binary stars (see Paper II). The moment mass transfer starts can then be determined by comparing the radius evolution of the most massive star with its Roche radius (Eggleton 1983). We predict the further evolution from the initial mass ratio of each binary system and whether the donor star had developed a deep convective envelope at the time of interaction. We assume that stable mass transfer occurs in systems with an initial mass ratio larger than a critical value ($q_{\rm crit,\,MS} = 0.65$ and $q_{\rm crit,\,HG} = 0.4$ for interaction initiated on the main-sequence and Hertzsprung gap following de Mink et al. 2007, and Hurley et al. 2002, respectively). For systems with a smaller initial mass ratio than the critical value and systems which have donor stars that have a deep convective envelope, we assume that a common envelope develops. We use the classical α-prescription to determine whether the common envelope is successfully ejected or not (Webbink 1984). For this, we assume $\lambda_{\rm CE} = 0.5$, which is average for Hertzsprung gap stars (see Appendix E of Izzard 2004) and describes how strongly the envelope is bound to the core of the star (Dewi & Tauris 2000; Tauris & Dewi 2001). We employ a standard value for the efficiency of the ejection of the common envelope, $\alpha_{\rm CE} = 1$ (see e.g., Hurley et al. 2002). We assume that the stars coalesce if either the core of the donor star or the companion star fills their Roche-lobe during the in-spiral inside the common envelope. It is likely that mass transfer within a common envelope leads to coalescence since the stars spiral closer together due to friction from the surrounding material. For the radii, we interpolate the zero-age main-sequence radius for the radius of the accretor star and the radii for the stripped stars (see Table 1 of Paper II). In cases when the accretor star has lower mass than our lowest mass model, we extrapolate to smaller radii.

We assign masses, times of envelope-stripping, and duration of the stripped phases by interpolating between the initial masses of the evolutionary models (see Sect. 2.1). In the same way, we also assign spectra and emission rates of ionizing photons. This approach neglects that Case A type mass transfer can result in somewhat lower mass stripped stars (see e.g., Pols 1994), but this evolutionary channel is responsible for less than a fourth of the total number of formed stripped stars and, therefore, is the total effect small.

We consider two different star-formation histories. The first is an instantaneous starburst with initially $10^6\,M_{\odot}$ of mass in stars. The second is a population in which stars form at a constant rate of $1\,M_{\odot}\,{\rm yr}^{-1}$. For the case of continuous star-formation, we use the predictions for the co-eval stellar population and convolve the spectral energy distribution and emission rates of ionizing photons over time. We perform the convolution every 1 Myr, which produces stochastic effects expected for a constant star-formation rate of $1\,M_{\odot}\,{\rm yr}^{-1}$.

2.3. Including the contribution from stripped stars to the model of a full stellar population

In the previous section, we described how we model the radiative contribution from stripped stars. To model the radiation from a realistic population, we also need to model the contribution of the remainder of the population, which includes single stars and stars in binary systems that have not yet interacted.

Starburst99 provides well-established models for the integrated spectra of stellar populations, including models of main-sequence stars, giant stars, and stars in more evolved stages of the stellar life (Leitherer et al. 1999, 2010). Most of the stars in a stellar population are main-sequence stars that have not yet interacted. Binary interaction primarily occurs at later evolutionary stages as the stars expand significantly after central hydrogen exhaustion and only mildly during the main-sequence. Starburst99 thus constitutes a fair approximation for stars that have not interacted with a binary companion. However, including stripped stars implies that there should be fewer giant stars as a fraction of them have become stripped. Moreover, the companions to stripped stars are expected to have accreted material and thus become more massive and somewhat rejuvenated. This leads to a slight increase in the radiation in optical and UV wavelengths since the mass-gaining star, in most cases, is a main-sequence star. We expect the total effect from mass-gainers and the lack of giant stars on the emission in the optical and UV wavelengths to be small, compared to the total emission from the full stellar population.

We use the combination of models from Starburst99 and our model for the contribution from stripped stars to repre-

sent the radiation of a full stellar population in which stripped stars are formed. We make our models publicly available as an add-on to the Starburst99 online interface[2], providing the addition from stripped stars to the spectral energy distribution, the emission rates of H I-, He I-, and He II-ionizing photons, and the high-resolution UV and optical spectra. Here, we use Starburst99 models without stellar rotation (cf. Levesque et al. 2012) and for metallicities Z = 0.014, 0.008, 0.002, and 0.001. We consider the combination to be a good assumption for radiation with wavelengths shorter than ∼ 5000 Å. For the model to be accurate at longer wavelengths, we would need to decrease the radiation from giant stars to compensate for stars that we assume have become stripped. Giant stars emit their radiation primarily at wavelengths longer than ∼ 5000 Å. We expect the decrement of radiation at these long wavelengths to be at maximum about 30%. This is approximately the fraction of massive stars that get stripped (Sana et al. 2012) and thus the fraction of giant stars that should be missing. This topic is beyond the scope of this paper, but we hope to address it more in detail at a later stage.

3. The impact of stripped stars on the spectral energy distribution

In this section, we describe the effect of stripped stars on the total spectral energy distribution of a stellar population. Although the contribution from stripped stars to the total bolometric luminosity is small, the hard, ionizing spectra of stripped stars do significantly change the shape of the spectral energy distribution. The differences mainly occur in the extreme ultraviolet. We discuss the effects for co-eval stellar populations in Sect. 3.1 and for the case of continuous star-formation in Sect. 3.2.

3.1. Predictions for co-eval stellar populations

Figure 1 shows how the spectral energy distribution is affected by the presence of stripped stars. The panels of the figure show snapshots taken 3, 11, 20, 50, 100, and 800 Myr after an instantaneous starburst of 10^6 $M_\odot$, assuming solar metallicity.

Stripped stars dominate the ionizing output from the stellar population after about 10 Myr and up to at least 100 Myr. At 3 Myr after starburst, shown in Fig. 1a, the ionizing radiation originates from massive main-sequence stars. Stars stripped in binaries are not yet present, because it takes time for them to form. Their progenitors, the donor stars, need time to evolve and swell up to fill their Roche-lobe. Stripped stars are therefore formed with a delay corresponding roughly to the main-sequence lifetime of the progenitor star. For a 20 $M_\odot$ progenitor star, the main-sequence lifetime, and thus the delay with which stripped stars with such progenitors form, is about 10 Myr. Also, stars that initiate mass transfer during the main-sequence evolution result in stripped stars after a time delay corresponding to the main-sequence lifetime of the donor star. The reason for this is that the mass transfer rate is slow during the main-sequence evolution and it is not terminated until central hydrogen depletion is reached.

Stars stripped in binaries are created over an extended period of time. The main-sequence lifetime, and therefore the time delay with which stripped stars are created, varies with the mass of the progenitor star. The stars that form stripped stars 11, 20, 50, 100, and 800 Myr after starburst have initial masses of about 18, 12, 7, 5, and 2 $M_\odot$. The resulting stripped stars have masses

[2] www.stsci.edu/science/starburst99/

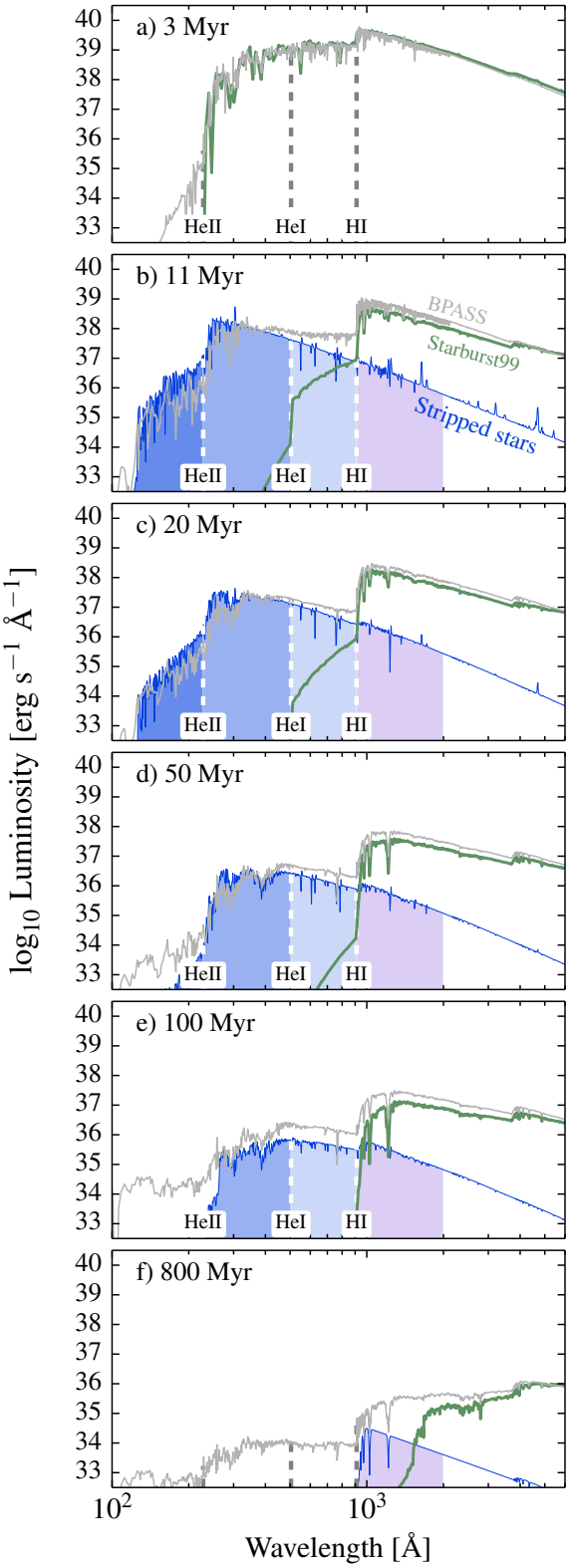

Fig. 1: The spectral energy distribution of a co-eval stellar population is shown, highlighting the contribution from stripped stars (blue line) using high-resolution spectra. The parts of the spectra that are H I-, He I-, and He II-ionizing are shaded in blue, while the UV is shaded in purple. For comparison, we show the spectral energy distribution of a population containing only single stars using Starburst99 (green line), which can be interpreted as the contribution from the remaining stars in the stellar population. We also show the predictions from BPASS (gray line), where the effects of binary interaction are included. The panels correspond to different times after the instantaneous starburst of 10^6 $M_\odot$. The model shown here assumes solar metallicity (see Appendix A for lower metallicity models).

of about 7, 4, 2, 1, and 0.5 $M_\odot$, respectively. The mass range of the stripped stars that are present at each point in time is small since the duration of the stripped phase is about 10 % of the main-sequence lifetime of the progenitor star and thus the time delay with which they are created. The temperature of stripped stars decreases with decreasing stellar mass as seen in Table 1 of Paper II, which shows that a 7 $M_\odot$ WR star has a temperature of 100 000 K, while a 1 $M_\odot$ subdwarf has a temperature of 40 000 K. This decrease in temperature causes their contribution to the integrated spectrum to become softer with time as the mass of the stripped stars that are present decreases.

As time proceeds, the number of stripped stars in a population increases. After ~ 10 Myr, the number of stripped stars present in a 10^6 $M_\odot$ co-eval stellar population is about 100, while after ~ 1 Gyr, we expect more than 500 stripped stars. Despite the increase in their total numbers with time, we find that the total bolometric luminosity produced by stripped stars decreases. This is because the luminosity of individual stripped stars is a steep function of mass.

About 500 Myr after starburst, the stripped stars no longer significantly contribute with ionizing photons, according to our models. The reason for this is that the stripped stars that are still present at these late times are subdwarfs. These subdwarfs are affected by diffusion processes, which alter their surface composition and structure (for a discussion see Sect. 3 of Paper II). The result is an increase of the abundance of hydrogen at their surfaces, which creates a sharp cut-off of the spectral energy distribution at the Lyman limit. The integrated spectra are still significantly different from what is expected for a population of single stars, see panel f of Fig. 1. At these late times, we expect that white dwarfs contribute with ionizing radiation (Panagia & Terzian 1984). However, more detailed modeling is needed to further understand the relative contributions of ionizing photons in late starbursts.

For comparison, we also show the spectral energy distributions predicted by the BPASS models in Fig. 1. We use version 2.1 of BPASS (*Kiwi*, Eldridge et al. 2017), which assumes that all stars are born in binary systems that have initial periods that are distributed evenly in log-space. We further choose to compare with the BPASS models that assume a similar slope of the IMF ($\alpha = -2.35$) as our models and that have the same mass limits as we assume. The BPASS predictions for the shape of the ionizing part of the spectral energy distribution match well with our predictions for populations younger than about 50 Myr. After this time, the BPASS models predict that the ionizing radiation is harder than what we find in our simulations. The reason is likely the adopted atmosphere models for central stars in planetary nebulae in BPASS, which are represented by hot WR star models (Gräfener et al. 2002).

The effect of metallicity on the shape of the spectral energy distribution is relatively small. At lower metallicity, stripped stars are slightly cooler (see Paper I for a discussion), which means that the ionizing part of the spectral energy distribution is slightly softer. However, the effects are small. The first notable differences occur at low metallicities, when $Z < 0.002$, see Fig. A.1.

3.2. Predictions for continuous star-formation

In Sect. 3.1 we showed that, for co-eval stellar populations, stripped stars make a distinct contribution to the ionizing spectra at late times, while massive main-sequence stars dominate at early times.

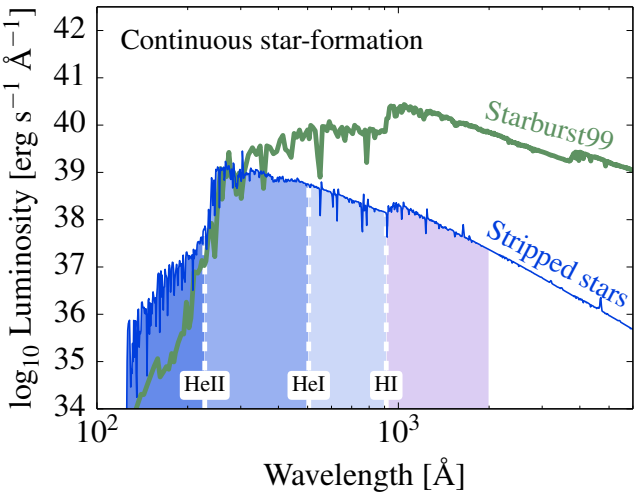

Fig. 2: The spectral energy distribution of a stellar population in which star-formation has taken place at a constant rate of 1 $M_\odot$ yr^{-1} for 500 Myr. Otherwise similar to Fig. 1. We show models with solar metallicity.

In Fig. 2, we show the integrated spectrum for the idealized case of constant star formation. The spectrum is for a population in which stars have formed at a constant rate of 1 $M_\odot$ yr^{-1}, and for a prolonged period of time, here chosen to be 500 Myr. At this time, the ionizing spectrum has reached equilibrium. The figure shows that the spectrum is heavily dominated by single stars at almost the entire wavelength range. Also, the emission of H I-ionizing photons is dominated by massive stars. The contribution from stripped stars to the total bolometric luminosity is negligible. They only dominate the emission of the hardest He II-ionizing photons. Note that our predictions for this part of the spectrum are uncertain and depend on the treatment of the stellar winds.

Realistic stellar populations are not co-eval, but contain a mixture of ages and characterized by a star-formation history that varies over time. For more realistic star-formation histories, the relative contribution from stripped stars depends on the recent star-formation activity. For populations that formed stars at a significant rate in the very recent past, $\lesssim 10$ Myr, massive stars likely dominate the output of ionizing photons. For populations that did not form stars very recently, we expect stripped stars to play a significant role.

4. Impact on the budget of ionizing photons

In this section, we discuss the emission rates of ionizing photons: $Q_{0,\mathrm{pop}}$, $Q_{1,\mathrm{pop}}$, and $Q_{2,\mathrm{pop}}$ for H I-, He I-, and He II-ionizing photons, respectively. We use the common definition of the emission rate of ionizing photons as the number of emitted photons with wavelengths shorter than the ionization threshold of the considered atom or ion, which can be calculated from the emitted luminosity, L_λ, in the following way:

$$Q_i = \frac{1}{hc} \int_0^{\lambda_i} \lambda L_\lambda \, d\lambda, \tag{1}$$

where h is the Planck's constant, c is the speed of light, and the subscript i refers to the considered ion. This method provides a good approximation for the emission rates of ionizing photons if the surrounding medium is sufficiently dense. The probability

that an ionizing photon will lead to ionization once it encounters an atom or ion is decreasing with increasing photon energy (Osterbrock & Ferland 2006). This decreasing ionization probability gives rise to a 100 times longer mean-free path for a photon with a wavelength of 228 Å compared to one of 912 Å in a medium containing only hydrogen (the mean-free path can be expressed as $\langle l \rangle = 1/(n\,\sigma)$, where n is the number density of the surrounding medium and σ is the ionization cross-section, which is wavelength dependent in the following way for hydrogen: $\sigma = \sigma_0(\lambda_0/\lambda)^3$). In a typical density for H II regions of 10^2 cm^{-2}, we calculate that these mean-free paths are of order 0.0005 pc and 0.05 pc, which are negligible length-scales in terms of the size of star-forming regions. We, therefore, consider the definition of the emission rates of ionizing photons as a realistic assumption.

We compare the expected contribution from the stripped stars with that from the massive single stars in the same stellar population. For this comparison, we use Starburst99 to represent the emission from the massive stars, as described in Sect. 2.3. We also show the predictions from the BPASS models.

4.1. Predictions for co-eval stellar populations

In Fig. 3a, we show the emission rate of H I-ionizing photons for a co-eval stellar population as a function of time after starburst. The massive stars in the stellar population primarily emit their H I-ionizing radiation during the first 5 Myr. Stripped stars play a significant role at later times.

At $\sim$ 10 Myr, when the first stripped stars have been created in our simulations, they emit ionizing photons with a rate of $\sim 10^{51}$ photons per second for a burst of $10^6\,M_\odot$ formed stars. This is an emission rate of about a factor of ten higher than what massive single stars produce at that time. About 100 Myr after starburst, the emission rate of H I-ionizing photons from stripped stars has decreased to $\sim 10^{49}$ s^{-1}, which corresponds to the typical emission rate of one WR-star or one massive O-star (Smith et al. 2002; Martins et al. 2005; Groh et al. 2014) and is several orders of magnitudes higher than expected from single stars. The emission of H I-ionizing photons keeps decreasing with time, and the trend suddenly steepens around 300 Myr. This is because the stripped stars that are present in the population are subdwarfs that have hydrogen-rich surfaces as a result of diffusion processes, as we discussed briefly in Sect. 3.1, see also Sect. 3 of Paper II. This results in a sharper Lyman cut-off in their spectra and thus a drop-off in the contribution of H I-ionizing photons. After $\sim$ 1 Gyr, the total ionizing emission rate is similar to that of one early B-type star ($Q_{0,\rm pop} \sim 10^{45}$ s^{-1}, cf. Smith et al. 2002).

Metallicity does not significantly affect the emission rate of H I-ionizing photons from stripped stars, as can be seen from the width of the shading in Fig. 3a. Because stripped stars have high temperatures ($T_{\rm eff} > 20\,000$ K) at all metallicities, the radiation peaks in the H I-ionizing wavelengths and $Q_{0,\rm pop}$ is, therefore, less dependent on metallicity. For stripped stars with progenitor masses that are lower than about $4\,M_\odot$, the emission rate of H I-ionizing photons increases with decreasing metallicity. However, because the time of stripping and duration of the stripped phase decreases with decreasing metallicity, the total emission rate of H I-ionizing photons from stripped stars in a population remains similar. The impact of metallicity on the H I-ionizing emission from main-sequence stars is larger than for stripped stars. The H I-ionizing emission rate from massive stars increases by up to a factor of five when metallicity is lowered. The boost of ionizing photons at late times due to the presence of stripped stars is independent of metallicity.

For comparison, we also show predictions from the BPASS models in Fig. 3a. They closely follow the predictions of Starburst99 during the first 5 Myr but show a boost of ionizing photons at later times, similar to our models of stripped stars (see also Stanway et al. 2016 and Wofford et al. 2016). Our predictions for the contribution of stripped stars follow the trend of the BPASS models after 10 Myr.The BPASS models predict a shallower decrease after $\sim$ 300 Myr compared to our models. We expect that this is due to differences in how we treat the atmospheres of stars in binary systems.

Stripped stars emit He I-ionizing photons at a rate that is about five times lower than that of H I-ionizing photons. In Fig. 1 the emitted luminosities appear to be of similar order for H I- and He I-ionizing radiation. However, the difference in the emission rates of He I- and H I-ionizing photons is larger since photons with shorter wavelengths are more energetic. The difference in emission rates of He I- and H I-ionizing photons can be seen by comparing the panels b and a in Fig. 3. The diagrams show that the decline of $Q_{1,\rm pop}$ closely follows that of $Q_{0,\rm pop}$. This is because the temperature of the stripped stars that are responsible for the ionizing emission does not change sufficiently to significantly affect the relative emission of He I- to H I-ionizing photons.

Once they are formed, stripped stars dominate the emission of He I-ionizing photons. The He I-ionizing emission rate predicted for single stars by Starburst99 decreases much more steeply with time than it does for stripped stars. Comparing to the emission of He I-ionizing photons from the main-sequence and WR stars, we see that stripped stars boost the emission rate by four orders of magnitudes already 10 Myr after starburst.

Changing the metallicity does not significantly alter the emission rate of He I-ionizing photons from stripped stars. At late times, around 300 Myr the evolution of $Q_{1,\rm pop}$ shows a feature, a temporary rise of the emission rate. The predictions for different metallicities deviate in this region as can be seen from the spread in the shading. This feature originates in the treatment of diffusion processes in surface layers of subdwarfs as discussed earlier.

The prediction of $Q_{1,\rm pop}$ from BPASS closely follows the predictions from stripped stars between 10 and 100 Myr after starburst. At early times, $\lesssim$ 5 Myr, we see that the predictions from BPASS closely follow those from Starburst99 at solar metallicity. However, for low metallicities, $Z \lesssim 0.002$, the BPASS models show an increase at these early times. The increase is particularly prominent between 3 and 20 Myr after starburst. This is a result of the treatment of stars that have gained mass or merged through binary interaction, causing them to rotate rapidly. Rapid rotation is thought to give rise to mixing processes in the stellar interior, causing the stars to evolve chemically homogeneously (Maeder 1987; Yoon & Langer 2005; Cantiello et al. 2007). Chemically homogeneous stars are thought to be very hot and bright and, if they exist, they can contribute with a significant amount of ionizing photons (Brott et al. 2011; Köhler et al. 2015; Szécsi et al. 2015; Kubátová et al. 2018).

Other sources that could affect the emission of H I-ionizing photons from stellar populations are white dwarfs (Panagia & Terzian 1984), rejuvenated mass-gainers (Chen & Han 2009; de Mink et al. 2014), and central stars in planetary nebulae or post-AGB stars (e.g., Miller Bertolami 2016).

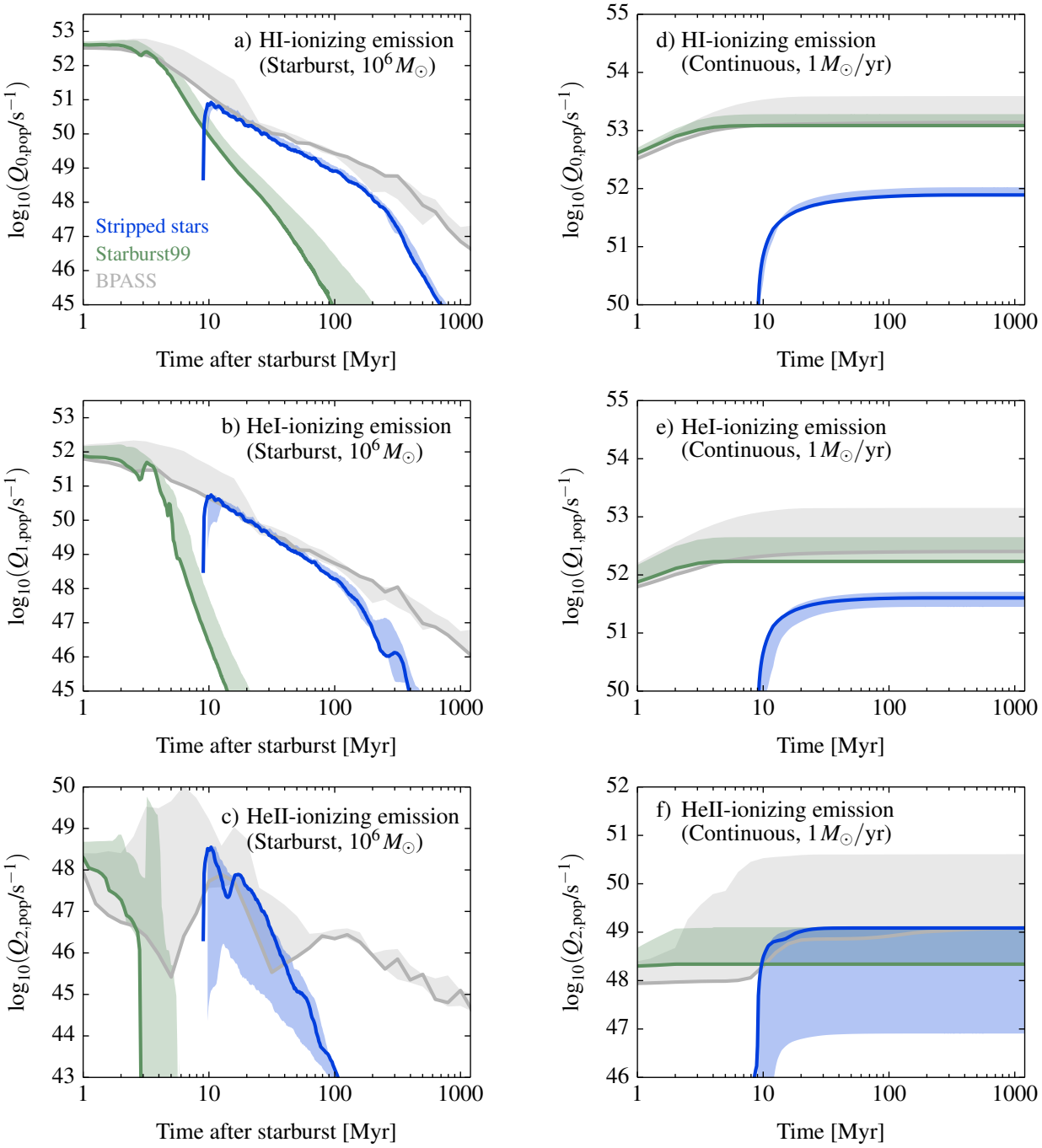

Fig. 3: The emission rates of ionizing photons from stellar populations as a function of time. The contribution from stripped stars is shown in blue, while green represents the contribution from the massive main sequence and WR stars in the stellar population (models from Starburst99, see Sect. 2.3). For reference, we show the predictions from BPASS models in which binary interactions are included using gray color. The solid lines correspond to the predictions from a population with solar metallicity, while the shaded regions of the same color represent the effects that lowering the metallicity has. The left column shows the emission rates from a co-eval stellar population with initially $10^6\,M_\odot$ in stars, and the right column shows the emission rates from a stellar population in which stars form at the constant rate of $1\,M_\odot\,\mathrm{yr}^{-1}$. The top, middle, and bottom rows show the emission rates of H I-, He I-, and He II-ionizing photons, respectively ($Q_{0,\mathrm{pop}}$, $Q_{1,\mathrm{pop}}$, and $Q_{2,\mathrm{pop}}$).

Our models predict that stripped stars are important contributors of the He II-ionizing photons emitted by stellar populations. Figure 3c shows that stripped stars reach emission rates of $\sim 10^{48.5}$ s^{-1}, which is similar to the emission rates from massive stars. Stripped stars maintain their high emission rate for longer because of their longer lifetimes and because they form from progenitors with a range of ages. The He II-ionizing emission is strongly temperature dependent. The decline of He II-ionizing emission with time is, therefore, steeper for $Q_{2,\mathrm{pop}}$ than for $Q_{0,\mathrm{pop}}$ or $Q_{1,\mathrm{pop}}$. After about 50 Myr, the emission rate of He II-ionizing photons from stripped stars falls below to 10^{45} s^{-1}.

Metallicity affects the emission rate of He II-ionizing photons from stripped stars, causing variations that span two orders of magnitude. The largest deviation occurs at the lowest metallicities, where we find that the stripping process fails to remove all the hydrogen, resulting in cooler stars (Paper I, Yoon et al.

2017). The emission rate of He II-ionizing photons is determined in the steep Wien-part of the stellar spectrum, meaning that a small shift in temperature results in a large shift in $Q_{2,\mathrm{pop}}$. The emission rate of He II-ionizing photons is also dependent on parameters of the stellar wind and can increase by several orders of magnitudes if, for example, the mass-loss rate is just a few factors lower (Paper I).

A feature in the otherwise smooth decline of $Q_{2,\mathrm{pop}}$ for stripped stars is seen in Fig. 3c about 15 Myr after starburst. This feature occurs because of the change of the treatment of wind clumping in the atmospheres of the stripped stars (see Paper II for details). Future detailed spectral analysis of observed stripped stars is necessary to constrain the properties of the stellar winds.

The BPASS predictions for $Q_{2,\mathrm{pop}}$ roughly follow the predictions of Starburst99 for the first $\sim$ 3 Myr. Between 10 and 50 Myr, they are consistent with our predictions for stripped stars. After that, BPASS predicts an emission rate that is several orders of magnitude higher and that stays high for the remaining considered time, probably because of the adopted atmosphere models for central stars in planetary nebulae. The models of BPASS predict that metallicity variations give rise to a large range of values for $Q_{2,\mathrm{pop}}$ before about 10 Myr has passed. Similar to the case of $Q_{1,\mathrm{pop}}$, we believe that these variations are due to rapidly rotating stars. Other types of stars that could play important roles as emitters of He II-ionizing photons are accreting white dwarfs or X-ray binaries (Chen et al. 2015; Fragos et al. 2013; Madau & Fragos 2017). These binaries reside in late evolutionary stages of interacting binaries, where one star has already died, possibly after interaction already occurred, and the second star now fills its Roche-lobe and transfers material to the compact object.

4.2. Predictions for continuous star-formation

We show the predicted emission rates of ionizing photons for continuous star-formation in Fig. 3d, e, and f. Once equilibrium is reached, stripped stars emit H I-ionizing photons at a rate of $10^{51.8}$ s^{-1}. This is about 5 % of the emission rate from massive stars ($10^{53.1}$ s^{-1}). As Fig. 3d shows, the massive stars dominate the emission of H I-ionizing photons in the case of continuous star-formation.

Stripped stars emit He I-ionizing photons at a rate that is about five times lower than the emission rate from massive stars. The contribution from stripped stars corresponds to about 15 % of the total stellar emission of He I-ionizing photons. Depending on the assumed metallicity, the contribution varies somewhat (between 10-20 %). At lower metallicity, the massive main sequence stars are hotter and therefore contribute with a larger fraction compared to the stripped stars.

The emission of He II-ionizing photons shown in Fig. 3f is dominated by the contribution from stripped stars as they emit about five times more He II-ionizing photons than the massive stars. Stripped stars reach emission rates of He II-ionizing photons of 10^{49} s^{-1}, while the massive stars only reach an emission rate of $10^{48.3}$ s^{-1}. We note that the emission rate of He II-ionizing photons is sensitive to metallicity variations. At very low metallicity ($Z \sim 0.0002$), the emission rate from stripped stars decreases by two orders of magnitude. Conversely, the emission rate from massive stars increases by a factor of five at very low metallicity.

5. Implications for observable quantities

In this section, we discuss the implications of accounting for stripped stars for various observable quantities commonly used to describe unresolved stellar populations. We summarize the values for the considered quantities in Table 1 at several snapshots after a starburst of $10^6\,M_\odot$ and also for continuous star-formation, taken after 500 Myr.

5.1. Diagnostics of the budget of ionizing photons

5.1.1. Production efficiency of ionizing photons, ξ_{ion}

The production efficiency of ionizing photons is a quantity that can be measured observationally. It relates the emission rates of ionizing photons to the UV luminosity and is, therefore, a parameter that describes the strength of the ionizing emission independent on the stellar mass or star-formation rate of the population. The production efficiency of hydrogen-ionizing photons has already been measured for a large number of unresolved stellar populations (Robertson et al. 2013; Stark et al. 2015; Bouwens et al. 2016; Matthee et al. 2017; Shivaei et al. 2018).

The production efficiency of ionizing photons is defined as follows:

$$\xi_{\mathrm{ion}} = \frac{Q_{\mathrm{pop}}}{L_\nu(1500\,\text{Å})}, \tag{2}$$

where Q_{pop} is the emission rate of ionizing photons and $L_\nu(1500\,\text{Å})$ is the luminosity at the wavelength 1500 Å in units of erg s^{-1} Hz^{-1}. We use $Q_{0,\mathrm{pop}}$, $Q_{1,\mathrm{pop}}$, and $Q_{2,\mathrm{pop}}$ in Eq. 2 to calculate the production efficiencies of H I-, He I-, and He II-ionizing photons, which we refer to as $\xi_{\mathrm{ion},0}$, $\xi_{\mathrm{ion},1}$, and $\xi_{\mathrm{ion},2}$, respectively. We average the UV luminosity between 1450 Å and 1550 Å to estimate the continuum luminosity and avoid fluctuations caused by spectral features.

For co-eval stellar populations, the ionizing radiation that stripped stars produce causes the production efficiencies of ionizing photons to remain at high values for much longer than what is predicted from single star populations. The integrated spectrum is harder if stripped stars are present, which can be recognized by comparing the production efficiency of H I-ionizing photons with either that of He I- or He II-ionizing photons. This is visualized in the hardness diagrams shown in Fig. 4.

Figure 4a shows that the same range of values for the production efficiency of H I-ionizing photons can be produced by either massive stars in a stellar population younger than 10 Myr or stripped stars in a stellar population that is up to ten times older (cf. Wilkins et al. 2016). In the figure, a clear separation is visible between a population that contains stripped stars and one that does not. The difference is due to the harder ionizing spectra that stripped stars introduce, which shift the production efficiencies of helium-ionizing photons to higher values relative to what is expected from a single star population. In the case of $\xi_{\mathrm{ion},2}$, the separation is several orders of magnitude. For continuous star-formation, the role of stripped stars is small for the production efficiencies of ionizing photons but could be relevant for $\xi_{\mathrm{ion},2}$, as can be seen from Fig. 4b and in Table 1.

For reference, we also show three distributions of measured $\xi_{\mathrm{ion},0}$ in observational samples of galaxies on top of the diagrams in Fig. 4. These samples are of distant galaxies with various classifications and span a range of redshifts (Bouwens et al. 2016; Matthee et al. 2017; Shivaei et al. 2018). The observed galaxies have a broad range of $\xi_{\mathrm{ion},0}$. For consistency, we chose to show the samples with the dust-correction made in the same way when

Table 1: Values of observable quantities for models of stellar populations including stripped stars. We use parentheses to show the values for single star populations (predicted by STARBURST99, Leitherer et al. 1999, 2010).

Co-eval stellar population ($10^6\,M_\odot$, $Z = 0.014$)									
Time [Myr]	$\log_{10}\,Q_{0,\mathrm{pop}}$ [s^{-1}]	$\log_{10}\,Q_{1,\mathrm{pop}}$ [s^{-1}]	$\log_{10}\,Q_{2,\mathrm{pop}}$ [s^{-1}]	$\log_{10}\,\xi_{\mathrm{ion},0}$ [$\mathrm{erg}^{-1}\,\mathrm{Hz}$]	$\log_{10}\,\xi_{\mathrm{ion},1}$ [$\mathrm{erg}^{-1}\,\mathrm{Hz}$]	$\log_{10}\,\xi_{\mathrm{ion},2}$ [$\mathrm{erg}^{-1}\,\mathrm{Hz}$]	$\log_{10}\,L_\nu(1500\text{Å})$ [$\mathrm{erg\,s^{-1}\,Hz^{-1}}$]	$\log_{10}\,U$	β
Section	4	4	4	5.1.1	5.1.1	5.1.1	5.1.1, 5.2	5.1.2	5.2
2	52.6 (52.6)	51.7 (51.7)	47.3 (47.3)	25.6 (25.6)	24.7 (24.7)	20.3 (20.3)	27.0 (27.0)	−2.0 (−2.0)	−2.97 (−2.97)
3	52.3 (52.3)	51.4 (51.4)	41.7 (41.7)	25.2 (25.2)	24.3 (24.3)	14.6 (14.6)	27.1 (27.1)	−2.1 (−2.1)	−2.5 (−2.5)
5	51.7 (51.7)	50.3 (50.3)	39.9 (39.9)	24.9 (24.9)	23.5 (23.5)	13.1 (13.1)	26.8 (26.8)	−2.3 (−2.3)	−2.41 (−2.41)
7	50.8 (50.8)	48.0 (48.0)	37.5 (37.5)	24.3 (24.3)	21.5 (21.5)	11.0 (11.0)	26.5 (26.5)	−2.6 (−2.6)	−2.41 (−2.41)
11	50.9 (49.8)	50.7 (46.0)	48.4 (–)	24.7 (23.6)	24.5 (19.9)	22.2 (–)	26.2 (26.2)	−2.6 (−3.0)	−2.32 (−2.31)
20	50.3 (48.6)	50.0 (43.4)	47.6 (–)	24.5 (22.8)	24.2 (17.6)	21.8 (–)	25.8 (25.8)	−2.8 (−3.4)	−2.21 (−2.2)
30	49.9 (47.9)	49.6 (41.5)	46.7 (–)	24.3 (22.3)	23.9 (15.9)	21.0 (–)	25.6 (25.6)	−2.9 (−3.6)	−2.02 (−2.01)
50	49.5 (46.7)	49.0 (39.8)	45.1 (–)	24.2 (21.4)	23.7 (14.4)	19.7 (–)	25.3 (25.3)	−3.1 (−4.0)	−1.83 (−1.82)
100	48.9 (44.9)	48.3 (37.7)	43.2 (–)	24.0 (19.9)	23.4 (12.8)	18.3 (–)	24.9 (24.9)	−3.2 (−4.6)	−1.51 (−1.49)
200	48.1 (42.8)	46.8 (–)	40.1 (–)	23.6 (18.3)	22.3 (–)	15.6 (–)	24.5 (24.5)	−3.5 (−5.3)	−1.2 (−1.17)
300	47.4 (41.5)	46.1 (–)	40.7 (–)	23.3 (17.4)	22.0 (–)	16.6 (–)	24.1 (24.1)	−3.8 (−5.7)	−0.41 (−0.31)
500	45.9 (39.6)	43.4 (–)	37.7 (–)	22.6 (16.3)	20.1 (–)	14.4 (–)	23.3 (23.3)	−4.3 (−6.4)	1.73 (2.54)
800	44.7 (36.7)	41.6 (–)	34.5 (–)	22.7 (15.3)	19.6 (–)	12.5 (–)	22.0 (21.4)	−4.6 (−7.3)	4.31 (9.73)
1000	44.2 (35.7)	40.8 (–)	33.8 (–)	22.5 (15.2)	19.1 (–)	12.1 (–)	21.7 (20.5)	−4.8 (−7.6)	4.58 (11.97)
Continuous star-formation ($1\,M_\odot$/year, $Z = 0.014$)									
Time [Myr]	$\log_{10}\,Q_{0,\mathrm{pop}}$ [s^{-1}]	$\log_{10}\,Q_{1,\mathrm{pop}}$ [s^{-1}]	$\log_{10}\,Q_{2,\mathrm{pop}}$ [s^{-1}]	$\log_{10}\,\xi_{\mathrm{ion},0}$ [$\mathrm{erg}^{-1}\,\mathrm{Hz}$]	$\log_{10}\,\xi_{\mathrm{ion},1}$ [$\mathrm{erg}^{-1}\,\mathrm{Hz}$]	$\log_{10}\,\xi_{\mathrm{ion},2}$ [$\mathrm{erg}^{-1}\,\mathrm{Hz}$]	$\log_{10}\,L_\nu(1500\text{Å})$ [$\mathrm{erg\,s^{-1}\,Hz^{-1}}$]	$\log_{10}\,U$	β
Section	4	4	4	5.1.1	5.1.1	5.1.1	5.1.1, 5.2	5.1.2	5.2
500	53.1 (53.1)	52.3 (52.2)	49.2 (48.3)	25.1 (25.1)	24.3 (24.3)	21.2 (20.4)	28.0 (28.0)	−1.8 (−1.9)	−2.27 (−2.27)

Notes. The presented quantities are the following. First, the emission rates of H I-, He I-, and He II-ionizing photons, which we refer to as $Q_{0,\mathrm{pop}}$, $Q_{1,\mathrm{pop}}$, and $Q_{2,\mathrm{pop}}$, respectively (Sect. 4). Then, the production efficiencies of H I-, He I-, and He II-ionizing photons, labelled $\xi_{\mathrm{ion},0}$, $\xi_{\mathrm{ion},1}$, and $\xi_{\mathrm{ion},2}$, respectively (Sect. 5.1.1). For calculating the production efficiencies, the UV luminosity of the following column was used (see Eq. 2 and also Sect. 5.2). The next column displays the ionization parameter, U (Sect. 5.1.2), and the last column the slope of the UV continuum, β (Sect. 5.2). We assume the gas density to be $n_\mathrm{H} = 100\,\mathrm{cm}^{-3}$ when calculating the ionization parameter. Snapshots for which no ionizing radiation was published are marked with '–'.

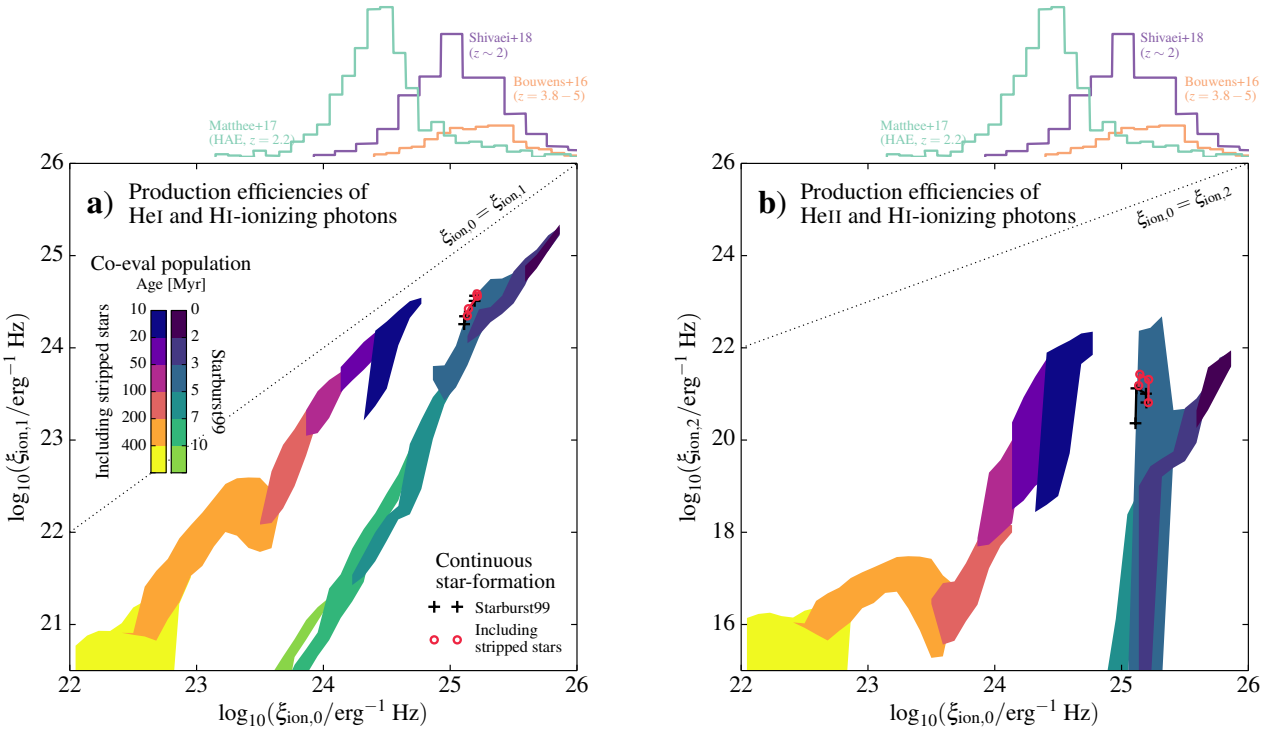

Fig. 4: Diagrams showing the hardness of the ionizing part of the spectrum of stellar populations, constructed by the production efficiencies of H I- and He I- (Panel a) or He II-ionizing photons (Panel b) ($\xi_{\rm ion,0}$, $\xi_{\rm ion,1}$, $\xi_{\rm ion,2}$). The colored regions represent the time spans indicated by the color bars for co-eval stellar populations and cover the predictions from all metallicities. Green shades show predictions for young, single star populations, while the purple and red shades represent the hardness of stellar populations in which stripped stars are included. The case of constant star-formation is shown with solid lines and markers (pluses in black for single stars and circles in red for when stripped stars are included), taken after 500 Myr. Above the diagrams, we show the distribution of measured $\xi_{\rm ion,0}$ for three samples of observed unresolved stellar populations from intermediate to high-redshift by Bouwens et al. (2016), Matthee et al. (2017), and Shivaei et al. (2018).

measuring the UV luminosity (assuming a Calzetti et al. 1994 slope for the dust extinction). We note that the method to account for the dust correction has an impact on the distribution of the estimated $\xi_{\rm ion,0}$ (Matthee et al. 2017, see also Hao et al. 2011; Murphy et al. 2011).

An interesting test of the underlying stellar population would be to measure the production efficiencies of helium-ionizing photons for observed galaxies, which would allow to place them individually in the hardness diagrams. We believe that this would provide a very valuable test for the models of stellar populations, and in particular for the impact of binary stellar evolution.

5.1.2. Ionization parameter, U

The ionization parameter is traditionally used to quantify the degree of ionization a stellar population causes on the surrounding nebula as it compares the flux of ionizing photons to the density of the surrounding gas (e.g., Osterbrock 1989). As a result, populations with the same ionization parameter typically show very similar nebular spectra even though they may have different stellar masses or star-formation rates (e.g., Dopita et al. 2000; Nakajima & Ouchi 2014).

We follow the standard definition of the ionization parameter, U, (e.g., Shields 1990, see also Kewley et al. 2013), where the isotropically emitted ionizing radiation from a central source is compared to the density of the gas surrounding the source:

$$U \equiv \frac{Q_{0,\rm pop}}{4\pi R_S^2 n_H c} = \frac{\alpha_B^{2/3}}{3^{2/3} c}\left(\frac{Q_{0,\rm pop}\epsilon^2 n_H}{4\pi}\right)^{1/3}. \quad (3)$$

In Eq. 3, n_H is the number density of hydrogen in the gas, ϵ is the volume filling factor of the gas, α_B is the recombination coefficient for hydrogen, and c is the speed of light. In the last equality of Eq. 3, we expanded the Strömgren radius, $R_S = [3\,Q_{0,\rm pop}/(4\pi n_H^2 \alpha_B \epsilon)]^{1/3}$ (Strömgren 1939). When calculating the ionization parameter, we account for clumping in the nebula by assuming $\epsilon = 0.1$, following Zastrow et al. (2013). We assume a typical gas temperature of 10 000 K, which leads $\alpha_B = 2.6 \times 10^{-13}$ cm^3 s^{-1} (Case B type recombination, Osterbrock & Ferland 2006). We adopt the emission rates of ionizing photons presented in Sect. 4 and assume a range of gas densities from $n_{\rm H} = 10$ to 10^4 cm^{-3}.

Our models show that stripped stars increase the ionization parameter for stellar populations in which star-formation has stopped at least 10 Myr ago, as shown in Fig. 5. The stripped stars allow the ionization parameter to remain at high values for an extended time period. In the case of constant star-formation, stripped stars increase U by about 2%.

The ionization parameter depends on the gas density and the emission rate of ionizing photons. The latter is closely related to the stellar mass in case of co-eval stellar populations and the star-formation rate in case of constant star-formation. We, therefore, compute the evolution of the ionization parameter for a range

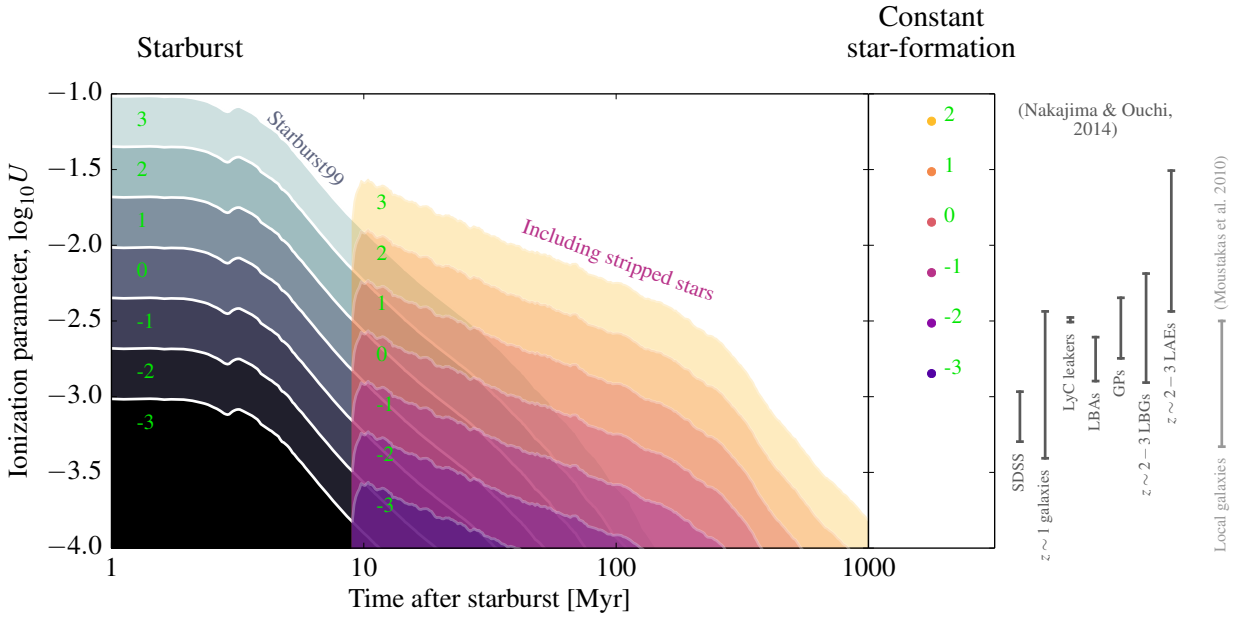

Explanation of the green labels.

Starburst	$10^3\ M_\odot$	$10^4\ M_\odot$	$10^5\ M_\odot$	$10^6\ M_\odot$	$10^7\ M_\odot$	$10^8\ M_\odot$	$10^9\ M_\odot$
Continuous	$0.001\ M_\odot\ \mathrm{yr}^{-1}$	$0.01\ M_\odot\ \mathrm{yr}^{-1}$	$0.1\ M_\odot\ \mathrm{yr}^{-1}$	$1\ M_\odot\ \mathrm{yr}^{-1}$	$10\ M_\odot\ \mathrm{yr}^{-1}$		
$10\ \mathrm{cm}^{-3}$	–	-3	-2	-1	0	1	2
$100\ \mathrm{cm}^{-3}$	-3	-2	-1	0	1	2	3
$1\,000\ \mathrm{cm}^{-3}$	-2	-1	0	1	2	3	–
$10\,000\ \mathrm{cm}^{-3}$	-1	0	1	2	3	–	–

Fig. 5: *Top:* The ionization parameter computed for co-eval stellar populations as a function of time and for constant star-formation, taken after 500 Myr. We show the predictions for stellar populations containing only single stars in gray shades and the model when stripped stars are included in purple shades. For constant star-formation, the contribution from stripped stars is about 2% and therefore we do not show the markers for single star populations as they overlap. We show measurements of the ionization parameter for groups of observed galaxies to the right of the diagram (Moustakas et al. 2010; Nakajima & Ouchi 2014). *Bottom:* The table explains which gas density and stellar mass for co-eval stellar populations that correspond to which contour in the diagram using numbers as labels. In the case of constant star-formation, the numbers are correlated with combinations of the gas density and star-formation rate instead.

of gas density, stellar mass, and star-formation rate combinations, as seen in Fig. 5. For reference, we show the measured ranges of several samples of observed galaxies as vertical bars on the right side of the figure (Moustakas et al. 2010; Nakajima & Ouchi 2014). These galaxies are grouped roughly according to their properties and redshift. The local galaxy samples are the SDSS galaxies, the Green Pea galaxies (GPs), the Lyman Continuum (LyC) leakers, and the Lyman-Break Analogs (LBAs) summarized by Nakajima & Ouchi (2014) together with the local galaxy sample presented by Moustakas et al. (2010). The samples of distant galaxies are the $z \sim 1$ galaxies, the Lyman Break Galaxies (LBGs) and the Lyman Alpha Emitters (LAEs) summarized in Nakajima & Ouchi (2014). The individual galaxies likely contain a mix of ages, however, it is also unlikely that they are subject to constant star-formation as in most cases a very low star-formation rate is inferred. As stripped stars prolong the time during which a stellar population can create ionizing photons, they could play an important role in shaping the distribution of ionization parameters found in the observed samples.

We do not expect that stripped stars contribute significantly to the ionizing emission from populations with very high measured values for the ionization parameter of $\log_{10} U \gtrsim -2$ as observed by, for example, Erb et al. (2010) and Leitherer et al. (2018). When stripped stars dominate the ionizing emission, such high ionization parameters require that the galaxy is of high mass ($\gtrsim 10^8\ M_\odot$) and that star-formation has halted about 10 Myr ago (see Fig. 5). Galaxies with such high ionization parameters are observed to have ongoing star-formation.

5.2. Impact on the UV luminosity and the UV continuum slope, β

The luminosity in the ultraviolet wavelengths, L_ν, has traditionally been used as a diagnostic for the star-formation rate of stellar populations (Kennicutt 1998) as the wavelength range is dominated by the emission from young and massive stars. Despite stripped stars are very hot, they do not significantly impact the UV luminosity in stellar populations that form stars at a constant

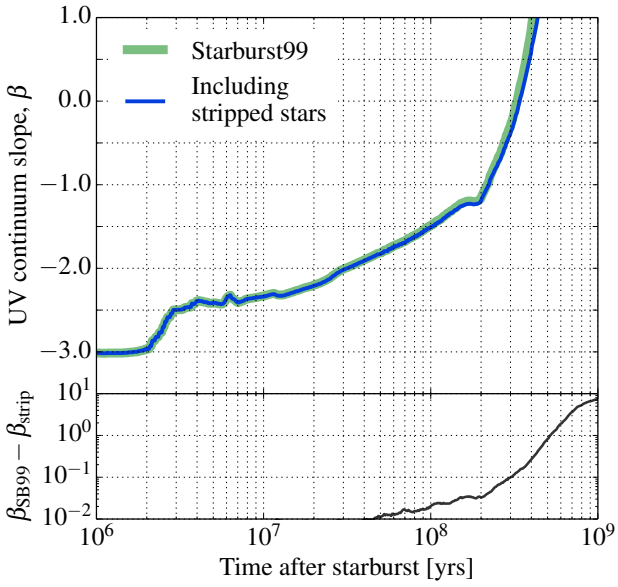

Fig. 6: The slope of the UV continuum, β, as a function of time for a co-eval stellar population. We show the UV slope for single star populations in green and for populations including stripped stars in blue. The bottom panel shows the difference between the two slopes. Up to 300 Myr years after starburst, the difference is smaller than 0.1.

rate or in which star-formation has halted less than 500 Myr ago. We display the results for L_ν at 1500 Å in Table 1.

The slope of the UV continuum, β, can be used to infer dust attenuation of stellar populations (e.g., Meurer et al. 1999). Similar to the UV luminosity, the slope of the UV continuum is not affected by the presence of stripped stars unless star-formation has halted more than about 100 Myr ago. To quantify the effect, we take the common approach and define the UV continuum slope as the exponent in a power-law: $F_\lambda \propto \lambda^\beta$, between 1250 Å and 2600 Å (Calzetti et al. 1994).

We find that stripped stars do not significantly affect the slope of the UV continuum if the slope is steep, $\beta \lesssim -0.5$, as seen in Fig. 6. For such cases, the UV is dominated by hot main-sequence stars. For shallower slopes of $\beta \sim -0.5$, stripped stars change β by at least 0.1, and for even shallower slopes stripped stars can dominate the UV radiation. This resembles the observed phenomenon called the UV-upturn (Burstein et al. 1988), which has been considered to originate from subdwarfs that are formed late after star-formation has ended, for example, through binary interaction in low-mass stars (Han et al. 2007). In our models, the UV slope becomes shallower with time for stellar populations in which stars are no longer forming. In the case of constant star-formation, the UV is dominated by radiation from massive stars and the effect of stripped stars on the UV slope is negligible. The effect of metallicity is small on both the UV luminosity and the slope of the UV continuum. We show the results for lower metallicity in Tables A.1, A.2 and A.3.

We conclude that both the UV luminosity and the slope of the UV continuum are un-affected by the presence of stripped stars in stellar populations in which star-formation is ongoing or that are younger than about 100 Myr. Therefore, in such stellar populations, the method of inferring the star-formation rate using the UV luminosity remains the same as well as inferring the dust attenuation using the UV continuum slope (cf. Reddy et al. 2018).

5.3. Impact on spectral features

We find that the stellar emission-line contribution from stripped stars is not distinguishable in the integrated spectrum of stellar populations. Their strongest emission feature is He II λ1640 and the equivalent width of this line increases at most by 1 Å when stripped stars are included. That is the case when the most massive stripped stars appear in co-eval and high-metallicity stellar populations. We note that higher wind mass-loss rates or slower stellar winds would increase the equivalent widths of the emission lines from stripped stars, as they are mainly formed by recombination in the stellar wind (see Sect. 2 and Paper II for a discussion).

The impact from stripped stars on the nebular spectrum is likely more interesting because their ionizing radiation affects the ionization state of the gas and thus also the spectral features emitted by the nebula. Nebular features are important diagnostics for the nature of observed galaxies and can, for example, be used to determine whether the ionizing source is stellar or quasar (Feltre et al. 2016; Gutkin et al. 2016, see also Stasińska et al. 2015). Detailed modeling of the nebular spectrum is needed to accurately estimate the impact of stripped stars and the topic of a forthcoming paper. Here, we discuss likely effects that stripped stars have on the nebula based on simple considerations of the hardness of the ionizing spectrum.

Figure 7 shows the shape of the ionizing part of the spectra of co-eval stellar populations compared to AGN (cf. Steidel et al. 2014; Stark et al. 2015; Feltre et al. 2016). We assume that the spectra of AGN are characterized by a power-law, $L_\nu \propto \nu^\alpha$, with a slope of $-2 < \alpha < -1.2$ (e.g., Feltre et al. 2016). The figure shows that the spectra from single star populations always are softer than that of AGN as they are characterized by steep spectral slopes of $\alpha \lesssim -2.5$ (see also D'Aloisio et al. 2018). When stripped stars are present, the ionizing spectrum for photon energies lower than about 50 eV is harder. The slope is even close to flat for stellar populations younger than 50 Myr. The spectrum becomes softer than what young and massive stars can produce first after more than 100 Myr after a starburst.

The ionizing part of the integrated spectrum is sufficiently hard when stripped stars are included for nebular oxygen to be ionized to O^{2+} and carbon to be ionized to C^{3+}, while the ionizing radiation from massive stars favors lower ionization stages such as O^+ and C^{2+}. The high ionization of carbon has been detected at high-redshift (e.g., the C IV λ1548 Å feature, Stark et al. 2015), making stripped stars interesting to consider as sources of such energetic photons. We also expect that stripped stars can give rise to high ratios of the nebular emission lines of O III to O II, which is a ratio used as an ionization measure and commonly labelled O32 (see e.g., Shapley et al. 2015; Strom et al. 2017, for observed distributions of O32). Full ionization of nebular helium is favored for the hard ionizing radiation of AGN compared to that of stellar populations. However, when stripped stars are included more He II-ionizing photons are produced than when only single stars are considered (see Sect. 4), which potentially could give rise to nebular He II features (cf. Kehrig et al. 2018).

We expect that stripped stars affect the location of stellar populations in the BPT diagram (Baldwin et al. 1981), which is a commonly used diagnostic diagram used to distinguish between star-forming galaxies and galaxies that host an AGN (Kewley et al. 2001; Kauffmann et al. 2003). For example, given the likely impact of stripped stars on the strength of O III lines, we expect that the ratio of [O III]/Hβ (the vertical axis of the BPT diagram) is affected. This is consistent with a recent study by Xiao et al.

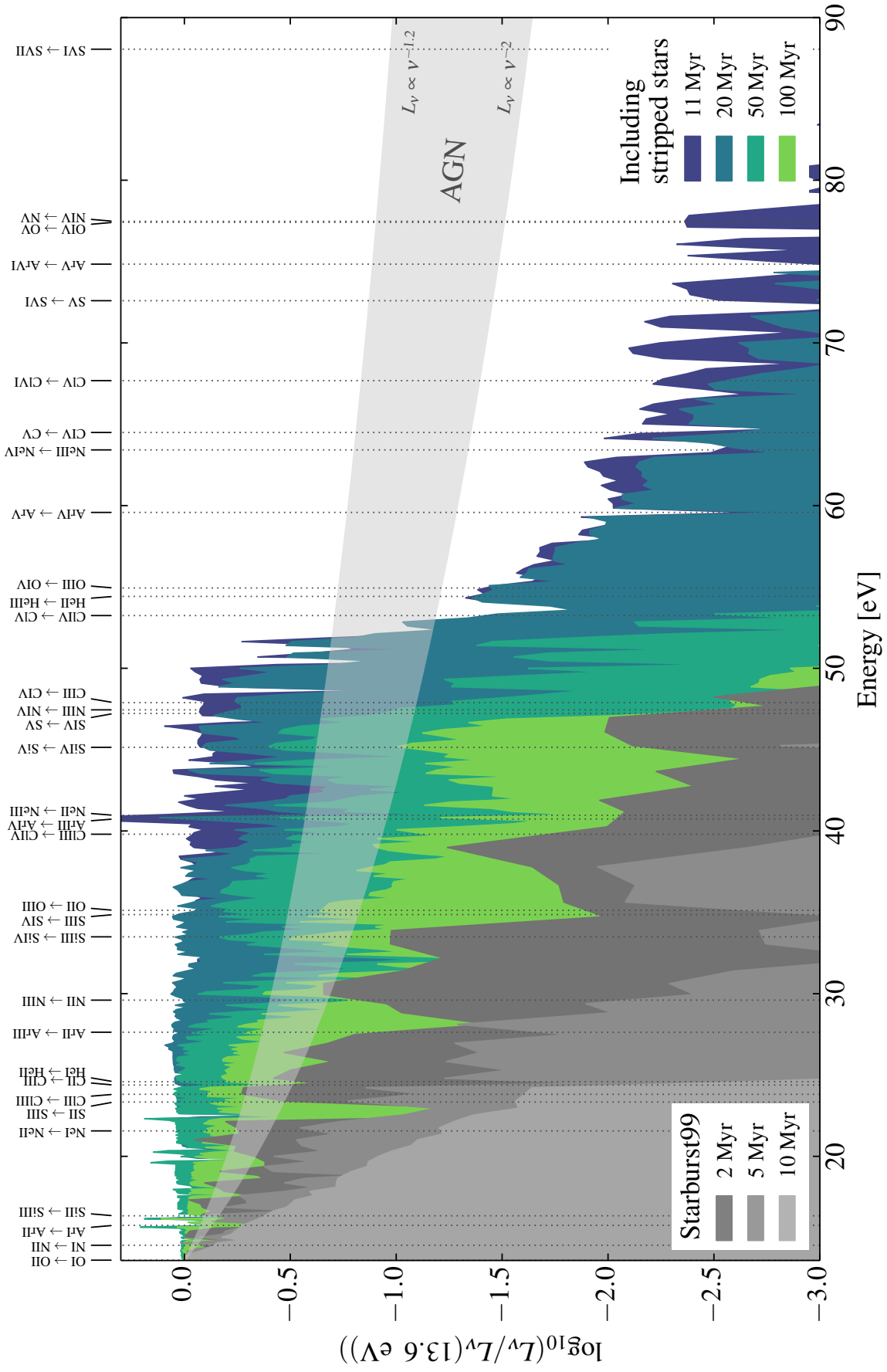

Fig. 7: The shape of the ionizing part of the spectra of co-eval stellar populations compared to that of AGN, shown by normalizing the spectra at the H I-ionizing threshold at the photon energy 13.6 eV. We use gray for the spectra of stellar populations that only contain single stars and green for spectra of stellar populations in which stripped stars are included. Expected spectral slopes for AGN are indicated in transparent gray. We mark the ionization thresholds of different ionization stages for a variety of elements above the figure.

(2018, see also Stanway et al. 2014) who used BPASS models and found that populations that contain stripped stars may be located in the same region as small dwarf galaxies with strong ionizing emission are found (e.g., the Green Pea galaxies, Cardamone et al. 2009, see also the low-mass galaxies of Shapley et al. 2015).

For lower metallicity, the spectra of massive stars become harder and the spectra of stripped stars become softer. However, a distinct difference in the hardness between the spectra of massive stars and those that stripped stars introduce is visible for metallicities larger than $Z = 0.0002$. This is visible in Fig. A.3, which shows figures analogous to Fig. 7, but for lower metallicities. In the case of $Z = 0.0002$, stripped stars produce as hard ionizing emission as the very youngest massive stars, which is interesting as the impact from stripped stars is present for up to 100 Myr, while the massive stars die after about 5 Myr.

In the case of constant star-formation, massive stars dominate and the result is a softer ionizing spectrum. Our models suggest that stripped stars primarily contribute with photons more energetic than 50 eV, but the increase is small and possibly difficult to distinguish.

5.3.1. Nebular Hα emission caused by stripped stars

Stripped stars produce photons capable of ionizing hydrogen and give rise to nebular Hα emission (Xiao et al. 2018). The contribution from stripped stars to nebular Hα is expected to be smaller than from massive stars for stellar populations in which stars form at a constant rate, since the line luminosity is related to the emission rate of H I-ionizing photons (see e.g., Leitherer & Heckman 1995; Schaerer 2003). However, in stellar populations in which star-formation has halted, stripped stars can be responsible the formation of nebular Hα.

Nebular Hα is often used to infer the star-formation rate of stellar populations as most H I-ionizing photons are produced by young and massive stars (Kennicutt 1998). Our models predict that this method is reliable unless star-formation has stopped more than about 10 Myr ago.

6. Summary & Conclusions

We have analyzed the radiative contribution from stars stripped in binaries to the spectral energy distribution and ionizing emission of stellar populations. To do this, we simulated a stellar population including a realistic fraction of binaries to estimate at what time stripped stars are expected to be present. For the spectra, we used our previously computed grid of custom-made atmosphere models (Paper II).

Our main focus is the ionizing emission since stripped stars emit the majority of their radiation in the ionizing wavelengths. They thus constitute a stellar source of ionizing photons that is neglected in models that only account for single stars. We compare the emission rates of hydrogen and helium ionizing photons from stripped stars to the emission rates from massive single main-sequence stars and WR stars as predicted by Starburst99. We also compare our results with predictions from the binary spectral synthesis code BPASS.

We quantify the effects of stripped stars on observable properties for co-eval stellar populations and continuous star-formation. These include the production efficiencies of hydrogen and helium ionizing photons ($\xi_{\rm ion,0}$, $\xi_{\rm ion,1}$, and $\xi_{\rm ion,2}$), the ionization parameter (U), the UV luminosity, and the UV-continuum slope (β). We find that the presence of stripped stars increases the hardness of the ionizing part of the integrated spectrum. The harder spectrum may be distinguishable when both the production efficiency of hydrogen and helium ionizing photons are inferred. It is also likely that the hard ionizing spectrum gives rise to a different ionization structure of the surrounding nebula and thus a characteristic combination of nebular emission lines.

Our main findings are the following:

1. Stripped stars are important as an additional stellar source of ionizing radiation. For co-eval stellar populations, stripped stars dominate the ionizing output by several orders of magnitude once they are created, which in our simulations is at an age of ~ 10 Myr. In the case of continuous star-formation their emission rates of H I-, He I-, and He II-ionizing photons reach levels as high as 5, 15, and 500% compared to what is expected from massive stars alone.

2. The ionizing emission from stripped stars is primarily important in stellar populations in which star-formation has recently halted. The reason is that stripped stars are created with a delay after the start of star-formation. The emission of ionizing photons from stripped stars is significant after about 10 Myr and up to 100 Myr after star-formation stopped.

3. Our models indicate that stripped stars only impact the integrated spectrum of a stellar population in the ionizing wavelengths.

4. Stripped stars introduce a characteristic hardness in the ionizing part of the spectral energy distribution. The effect on observable properties is not only an increase in the production efficiency of H I-ionizing photons ($\xi_{\rm ion,0}$), but a relatively larger increase in the production efficiency of He I- and He II-ionizing photons ($\xi_{\rm ion,1}$ and $\xi_{\rm ion,2}$). Current measurements of $\xi_{\rm ion,0}$ agree well with our predictions. We argue that future measurements of $\xi_{\rm ion,1}$ and $\xi_{\rm ion,2}$ will provide stringent tests for the theoretical models.

5. The presence of stripped stars in co-eval populations also affects the commonly used ionization parameter (U), causing it to remain between $-3.5 \lesssim \log_{10} U \lesssim -2.5$ for a few 100 Myr. This is a range that often is observed for stellar populations. In the case of continuous star-formation, stripped stars only affect the ionization parameter by up to 2%.

6. The ionizing radiation introduced by stripped stars is sufficiently hard to ionize the nebula to high ionization states, which potentially are visible via nebular emission lines if gas is still present at these times. Stripped stars likely have the largest relative impact on the nebular spectrum for stellar populations in which star-formation recently halted. In these cases, it is likely that the nebula reaches high ionization states, such as O^{2+}, C^{3+}, and possibly also fully ionized helium. Because of the hard, integrated spectrum, we expect high ratios of nebular emission of O III to O II (O32). This means that the location of the stellar population in the BPT diagram is affected as well (cf. Xiao et al. 2018).

7. Stripped stars do not significantly affect the UV luminosity or the slope of the UV continuum (β) in populations in which stars form at a constant rate or in populations that

are younger than ∼100 Myr. This means that in such populations, the UV luminosity can still be used as a reliable diagnostic for the star-formation rate and the UV continuum slope can be used to make inferences about dust attenuation. However, in co-eval populations with ages between about 200 Myr and 1 Gyr, stripped stars significantly affect or even dominate the output of UV radiation, which significantly affects the UV continuum slope. However, at this point the slope is already close to flat, $\beta \gtrsim -0.5$.

8. For co-eval stellar populations, metallicity only modestly affects the emission of ionizing photons from stripped stars. However, in the case of continuous star-formation, metallicity become more important. With lower metallicity, the stripped stars are cooler and their effect on the spectral hardness is therefore smaller. However, other products of binary interaction, such as rapidly spinning accretor stars, may still have large effects (cf. Eldridge et al. 2017).

Our models are publicly available on the CDS database, where we provide electronic tables with the contribution from stripped stars to the spectral energy distribution and to the emission rates of H I-, He I-, and He II-ionizing photons. Our models can also be obtained via the STARBURST99 online interface.

Acknowledgements. SdM has received funding under the European Union's Horizon 2020 research and innovation programme from the European Research Council (ERC) (Grant agreement No. 715063). JHG acknowledges support from the Irish Research Council New Foundations Award 206086.14414 'Physics of Supernovae and Stars'. This work made use of v2.1 of the Binary Population and Spectral Synthesis (BPASS) models as last described in Eldridge, Stanway et al. (2017).

References

Baldwin, J. A., Phillips, M. M., & Terlevich, R. 1981, PASP, 93, 5
Barkana, R. & Loeb, A. 2001, Phys. Rep., 349, 125
Belkus, H., Van Bever, J., Vanbeveren, D., & van Rensbergen, W. 2003, A&A, 400, 429
Bestenlehner, J. M., Gräfener, G., Vink, J. S., et al. 2014, A&A, 570, A38
Bouwens, R. J., Smit, R., Labbé, I., et al. 2016, ApJ, 831, 176
Brott, I., de Mink, S. E., Cantiello, M., et al. 2011, A&A, 530, A115
Bruzual, G. & Charlot, S. 2003, MNRAS, 344, 1000
Burstein, D., Bertola, F., Buson, L. M., Faber, S. M., & Lauer, T. R. 1988, ApJ, 328, 440
Calzetti, D., Kinney, A. L., & Storchi-Bergmann, T. 1994, ApJ, 429, 582
Cantiello, M., Yoon, S.-C., Langer, N., & Livio, M. 2007, A&A, 465, L29
Cardamone, C., Schawinski, K., Sarzi, M., et al. 2009, MNRAS, 399, 1191
Charlot, S. & Longhetti, M. 2001, MNRAS, 323, 887
Chen, H.-L., Woods, T. E., Yungelson, L. R., Gilfanov, M., & Han, Z. 2015, MNRAS, 453, 3024
Chen, X. & Han, Z. 2009, MNRAS, 395, 1822
Chen, X. & Han, Z. 2010, Ap&SS, 329, 277
Chiosi, C. & Maeder, A. 1986, ARA&A, 24, 329
Chojnowski, S. D., Labadie-Bartz, J., Rivinius, T., et al. 2018, ArXiv e-prints [arXiv:1806.06843]
Claeys, J. S. W., de Mink, S. E., Pols, O. R., Eldridge, J. J., & Baes, M. 2011, A&A, 528, A131
Conroy, C. 2013, ARA&A, 51, 393
Crowther, P. A. 2007, ARA&A, 45, 177
Dale, J. E., Ercolano, B., & Bonnell, I. A. 2013, MNRAS, 431, 1062
D'Aloisio, A., McQuinn, M., Maupin, O., et al. 2018, ArXiv e-prints [arXiv:1807.09282]
de Mink, S. E., Pols, O. R., & Hilditch, R. W. 2007, A&A, 467, 1181
de Mink, S. E., Sana, H., Langer, N., Izzard, R. G., & Schneider, F. R. N. 2014, ApJ, 782, 7
Dewi, J. D. M. & Tauris, T. M. 2000, A&A, 360, 1043
Dopita, M. A., Kewley, L. J., Heisler, C. A., & Sutherland, R. S. 2000, ApJ, 542, 224
Eggleton, P. P. 1983, ApJ, 268, 368
Ekström, S., Georgy, C., Eggenberger, P., et al. 2012, A&A, 537, A146
Eldridge, J. J., Izzard, R. G., & Tout, C. A. 2008, MNRAS, 384, 1109
Eldridge, J. J. & Maund, J. R. 2016, MNRAS, 461, L117
Eldridge, J. J. & Stanway, E. R. 2009, MNRAS, 400, 1019
Eldridge, J. J. & Stanway, E. R. 2012, MNRAS, 419, 479
Eldridge, J. J. & Stanway, E. R. 2016, MNRAS, 462, 3302
Eldridge, J. J., Stanway, E. R., & Tang, P. N. 2018, ArXiv e-prints [arXiv:1807.07659]
Eldridge, J. J., Stanway, E. R., Xiao, L., et al. 2017, PASA, 34, e058
Erb, D. K., Pettini, M., Shapley, A. E., et al. 2010, ApJ, 719, 1168
Feltre, A., Charlot, S., & Gutkin, J. 2016, MNRAS, 456, 3354
Fioc, M. & Rocca-Volmerange, B. 1997, A&A, 326, 950
Fioc, M. & Rocca-Volmerange, B. 1999, ArXiv Astrophysics e-prints [astro-ph/9912179]
Fragos, T., Lehmer, B., Tremmel, M., et al. 2013, ApJ, 764, 41
Gardner, J. P., Mather, J. C., Clampin, M., et al. 2006, Space Sci. Rev., 123, 485
Gies, D. R., Bagnuolo, Jr., W. G., Ferrara, E. C., et al. 1998, ApJ, 493, 440
Götberg, Y., de Mink, S. E., & Groh, J. H. 2017, A&A, 608, A11
Götberg, Y., de Mink, S. E., Groh, J. H., et al. 2018, A&A, 615, A78
Gräfener, G., Koesterke, L., & Hamann, W.-R. 2002, A&A, 387, 244
Groh, J. H., Meynet, G., Ekström, S., & Georgy, C. 2014, A&A, 564, A30
Groh, J. H., Oliveira, A. S., & Steiner, J. E. 2008, A&A, 485, 245
Gutkin, J., Charlot, S., & Bruzual, G. 2016, MNRAS, 462, 1757
Han, Z., Podsiadlowski, P., & Lynas-Gray, A. 2010, Ap&SS, 329, 41
Han, Z., Podsiadlowski, P., & Lynas-Gray, A. E. 2007, MNRAS, 380, 1098
Han, Z., Podsiadlowski, P., Maxted, P. F. L., Marsh, T. R., & Ivanova, N. 2002, MNRAS, 336, 449
Hao, C.-N., Kennicutt, R. C., Johnson, B. D., et al. 2011, ApJ, 741, 124
Heber, U. 2016, PASP, 128, 082001
Hillier, D. J. 1990, A&A, 231, 116
Hillier, D. J. & Miller, D. L. 1998, ApJ, 496, 407
Hurley, J. R., Tout, C. A., & Pols, O. R. 2002, MNRAS, 329, 897
Ivanova, N. 2011, ApJ, 730, 76
Izzard, R. G. 2004, PhD thesis, University of Cambridge
Kauffmann, G., Heckman, T. M., Tremonti, C., et al. 2003, MNRAS, 346, 1055
Kehrig, C., Vílchez, J. M., Guerrero, M. A., et al. 2018, MNRAS
Kennicutt, Jr., R. C. 1998, ARA&A, 36, 189
Kewley, L. J., Dopita, M. A., Leitherer, C., et al. 2013, ApJ, 774, 100
Kewley, L. J., Dopita, M. A., Sutherland, R. S., Heisler, C. A., & Trevena, J. 2001, ApJ, 556, 121
Kiminki, D. C. & Kobulnicky, H. A. 2012, ApJ, 751, 4
Kippenhahn, R. & Weigert, A. 1967, ZAp, 65, 251
Köhler, K., Langer, N., de Koter, A., et al. 2015, A&A, 573, A71
Kouwenhoven, M. B. N., Brown, A. G. A., Portegies Zwart, S. F., & Kaper, L. 2007, A&A, 474, 77
Kriek, M., Shapley, A. E., Reddy, N. A., et al. 2015, ApJS, 218, 15
Kroupa, P. 2001, MNRAS, 322, 231
Krtička, J., Kubát, J., & Krtičková, I. 2016, A&A, 593, A101
Krumholz, M. R., Matzner, C. D., & McKee, C. F. 2006, ApJ, 653, 361
Kubátová, B., Szécsi, D., Sander, A. A. C., et al. 2018, ArXiv e-prints [arXiv:1810.01267]
Lapi, A., Mancuso, C., Celotti, A., & Danese, L. 2017, ApJ, 835, 37
Le Borgne, D., Rocca-Volmerange, B., Prugniel, P., et al. 2004, A&A, 425, 881
Le Fèvre, O., Tasca, L. A. M., Cassata, P., et al. 2015, A&A, 576, A79
Leitherer, C., Byler, N., Lee, J. C., & Levesque, E. M. 2018, ApJ, 865, 55
Leitherer, C., Ekström, S., Meynet, G., et al. 2014, ApJS, 212, 14
Leitherer, C. & Heckman, T. M. 1995, ApJS, 96, 9
Leitherer, C., Ortiz Otálvaro, P. A., Bresolin, F., et al. 2010, ApJS, 189, 309
Leitherer, C., Schaerer, D., Goldader, J. D., et al. 1999, ApJS, 123, 3
Levesque, E. M., Leitherer, C., Ekstrom, S., Meynet, G., & Schaerer, D. 2012, ApJ, 751, 67
Li, Z., Zhang, L., & Liu, J. 2012, MNRAS, 424, 874
Madau, P. & Fragos, T. 2017, ApJ, 840, 39
Maeder, A. 1987, A&A, 178, 159
Martins, F., Schaerer, D., & Hillier, D. J. 2005, A&A, 436, 1049
Massey, P., Neugent, K. F., & Morrell, N. 2015, ApJ, 807, 81
Massey, P., Neugent, K. F., & Morrell, N. 2017, ApJ, 837, 122
Massey, P., Neugent, K. F., Morrell, N., & Hillier, D. J. 2014, ApJ, 788, 83
Matthee, J., Sobral, D., Best, P., et al. 2017, MNRAS, 465, 3637
Meurer, G. R., Heckman, T. M., & Calzetti, D. 1999, ApJ, 521, 64
Meynet, G. & Maeder, A. 2005, A&A, 429, 581
Miller Bertolami, M. M. 2016, A&A, 588, A25
Moe, M. & Di Stefano, R. 2017, ApJS, 230, 15
Moustakas, J., Kennicutt, Jr., R. C., Tremonti, C. A., et al. 2010, ApJS, 190, 233
Murphy, E. J., Condon, J. J., Schinnerer, E., et al. 2011, ApJ, 737, 67
Nakajima, K. & Ouchi, M. 2014, MNRAS, 442, 900
Nanayakkara, T., Glazebrook, K., Kacprzak, G. G., et al. 2016, ApJ, 828, 21
Neugent, K. F., Massey, P., Hillier, D. J., & Morrell, N. 2017, ApJ, 841, 20
Neugent, K. F., Massey, P., & Morrell, N. 2018, ArXiv e-prints [arXiv:1807.01209]
Nugis, T. & Lamers, H. J. G. L. M. 2000, A&A, 360, 227
Öpik, E. 1924, Publications of the Tartu Astrofizica Observatory, 25

Osterbrock, D. E. 1989, Astrophysics of gaseous nebulae and active galactic nuclei
Osterbrock, D. E. & Ferland, G. J. 2006, Astrophysics of gaseous nebulae and active galactic nuclei
Paczyński, B. 1967, Acta Astron., 17, 355
Paczynski, B. 1976, Symposium - International Astronomical Union, 73, 75
Panagia, N. & Terzian, Y. 1984, ApJ, 287, 315
Paquette, C., Pelletier, C., Fontaine, G., & Michaud, G. 1986, ApJS, 61, 177
Paxton, B., Bildsten, L., Dotter, A., et al. 2011, ApJS, 192, 3
Paxton, B., Cantiello, M., Arras, P., et al. 2013, ApJS, 208, 4
Paxton, B., Marchant, P., Schwab, J., et al. 2015, ApJS, 220, 15
Paxton, B., Schwab, J., Bauer, E. B., et al. 2018, ApJS, 234, 34
Peters, G. J., Gies, D. R., Grundstrom, E. D., & McSwain, M. V. 2008, ApJ, 686, 1280
Peters, G. J., Pewett, T. D., Gies, D. R., Touhami, Y. N., & Grundstrom, E. D. 2013, ApJ, 765, 2
Podsiadlowski, P., Joss, P. C., & Hsu, J. J. L. 1992, ApJ, 391, 246
Pols, O. R. 1994, A&A, 290
Reddy, N. A., Oesch, P. A., Bouwens, R. J., et al. 2018, ApJ, 853, 56
Robertson, B. E., Ellis, R. S., Dunlop, J. S., McLure, R. J., & Stark, D. P. 2010, Nature, 468, 49
Robertson, B. E., Furlanetto, S. R., Schneider, E., et al. 2013, ApJ, 768, 71
Rudie, G. C., Steidel, C. C., Trainor, R. F., et al. 2012, ApJ, 750, 67
Sana, H., de Mink, S. E., de Koter, A., et al. 2012, Science, 337, 444
Schaerer, D. 2003, A&A, 397, 527
Schneider, F. R. N., Izzard, R. G., Langer, N., & de Mink, S. E. 2015, ApJ, 805, 20
Schneider, F. R. N., Ramírez-Agudelo, O. H., Tramper, F., et al. 2018, ArXiv e-prints [arXiv:1807.03821]
Shapley, A. E., Reddy, N. A., Kriek, M., et al. 2015, ApJ, 801, 88
Shields, G. A. 1990, ARA&A, 28, 525
Shivaei, I., Reddy, N. A., Siana, B., et al. 2018, ApJ, 855, 42
Siess, L. & Lebreuilly, U. 2018, ArXiv e-prints [arXiv:1807.04008]
Smith, L. J., Norris, R. P. F., & Crowther, P. A. 2002, MNRAS, 337, 1309
Smith, N., Götberg, Y., & de Mink, S. E. 2018, MNRAS, 475, 772
Sravan, N., Marchant, P., & Kalogera, V. 2018, ArXiv e-prints [arXiv:1808.07580]
Stanway, E. R. & Eldridge, J. J. 2018, MNRAS, 479, 75
Stanway, E. R., Eldridge, J. J., & Becker, G. D. 2016, MNRAS, 456, 485
Stanway, E. R., Eldridge, J. J., Greis, S. M. L., et al. 2014, MNRAS, 444, 3466
Stark, D. P., Walth, G., Charlot, S., et al. 2015, MNRAS, 454, 1393
Stasińska, G., Costa-Duarte, M. V., Vale Asari, N., Cid Fernandes, R., & Sodré, L. 2015, MNRAS, 449, 559
Steidel, C. C., Bogosavlevic, M., Shapley, A. E., et al. 2018, ArXiv e-prints [arXiv:1805.06071]
Steidel, C. C., Rudie, G. C., Strom, A. L., et al. 2014, ApJ, 795, 165
Strom, A. L., Steidel, C. C., Rudie, G. C., et al. 2017, ApJ, 836, 164
Strömgren, B. 1939, ApJ, 89, 526
Szécsi, D., Langer, N., Yoon, S.-C., et al. 2015, A&A, 581, A15
Tauris, T. M. & Dewi, J. D. M. 2001, A&A, 369, 170
Thoul, A. A., Bahcall, J. N., & Loeb, A. 1994, ApJ, 421, 828
Treu, T., Schmidt, K. B., Brammer, G. B., et al. 2015, ApJ, 812, 114
Van Bever, J., Belkus, H., Vanbeveren, D., & Van Rensbergen, W. 1999, New A, 4, 173
Van Bever, J. & Vanbeveren, D. 2003, A&A, 400, 63
van der Linden, T. J. 1987, A&A, 178, 170
van Haaften, L. M., Nelemans, G., Voss, R., et al. 2013, A&A, 552, A69
Vanbeveren, D., de Grève, J. P., van Dessel, E. L., & de Loore, C. 1979, A&A, 73, 19
Vanbeveren, D., Van Bever, J., & Belkus, H. 2007, ApJ, 662, L107
Vink, J. S. 2017, A&A, 607, L8
Wang, L., Gies, D. R., & Peters, G. J. 2017, ApJ, 843, 60
Wang, L., Gies, D. R., & Peters, G. J. 2018, ApJ, 853, 156
Webbink, R. F. 1984, ApJ, 277, 355
Wellstein, S. & Langer, N. 1999, A&A, 350, 148
Wilkins, S. M., Feng, Y., Di-Matteo, T., et al. 2016, MNRAS, 458, L6
Wofford, A., Charlot, S., Bruzual, G., et al. 2016, MNRAS, 457, 4296
Xiao, L., Stanway, E. R., & Eldridge, J. J. 2018, MNRAS, 477, 904
Yoon, S.-C., Dessart, L., & Clocchiatti, A. 2017, ApJ, 840, 10
Yoon, S.-C. & Langer, N. 2005, A&A, 443, 643
Yoon, S.-C., Woosley, S. E., & Langer, N. 2010, ApJ, 725, 940
Zastrow, J., Oey, M. S., & Pellegrini, E. W. 2013, ApJ, 769, 94
Zhang, F., Han, Z., Li, L., & Hurley, J. R. 2004, A&A, 415, 117
Zhang, F., Li, L., Cheng, L., et al. 2015, MNRAS, 447, L21
Zhang, F., Li, L., Zhang, Y., Kang, X., & Han, Z. 2012, MNRAS, 421, 743

Appendix A: Effect of metallicity

Main-sequence stars are more luminous and hotter at low metallicity than at high metallicity. Their emission rates of ionizing photons therefore increase with decreasing metallicity. The emission rates of ionizing photons from stripped stars are also affected by their luminosity and effective temperature. The luminosity of stripped stars increases with lower metallicity, but the effective temperature decreases (Paper I; Paper II). The reason is primarily that envelope-stripping is less efficient when the metallicity is decreased, which leads to more hydrogen left after mass transfer and therefore lower temperatures. Here, we combine the models for stripped stars at metallicities $Z = 0.006$, 0.002, and 0.0002, with the models from Starburst99 for $Z = 0.008$, 0.002, and 0.001, respectively. We compare with the BPASS models with $Z = 0.006$, 0.002, and 0.0001.

We show the evolution of the contribution from stripped stars to the integrated spectrum of a co-eval stellar population in Fig. A.1. The figure shows that the emission from stripped stars becomes softer when metallicity decreases, while the emission from main-sequence stars becomes harder. As shown in Fig. 3, the total effect of metallicity on the emission from stripped stars is small for $Q_{0,\mathrm{pop}}$ and $Q_{1,\mathrm{pop}}$, but large for $Q_{2,\mathrm{pop}}$. The reason why the effect is large for $Q_{2,\mathrm{pop}}$ is that He II-ionizing photons are created in the steep Wien-part of the spectrum and the emission rate of He II-ionizing photons is therefore very sensitive to temperature variations.

The most striking differences between our predictions and those from BPASS occur at low metallicity. Around 10 Myr after starburst and for $Z \leq 0.002$, BPASS accounts for chemically homogeneous evolution for the accreting stars that were spun up during mass transfer (Eldridge et al. 2017). The result is that BPASS predicts higher emission rates of H I- and He I-ionizing photons than our models for stripped stars at low metallicity.

For continuous star-formation, we show the contribution from stripped stars to the spectral energy distribution in Fig. A.2 for the cases of lower metallicity. Comparing with Fig. 2, we find that the contribution from stripped stars is similar for $Z \gtrsim 0.002$, while the softer spectra of stripped stars are clearly visible at metallicity $Z = 0.0002$.

The hardness of the ionizing part of the integrated spectrum affects the nebular ionization, as discussed in Sect. 5.3. We show the ionizing part of the spectra of co-eval stellar populations at low metallicity in Fig. A.3. The spectra of main-sequence stars are seen to become harder and those of stripped stars to become softer with lower metallicity. At $Z = 0.0002$, the hardness is similar for a population containing stripped stars and at an age of 20 Myr as for a population of only 2 Myr that contains massive main-sequence stars. However, we note that the duration for which massive stars give rise to such hard ionizing spectra is significantly shorter than the duration stripped stars emit ionizing radiation.

As a complement to Fig. 7, we show the hardness of the ionizing part of the spectrum for a stellar population in which stars have formed at a constant rate for 500 Myr and with solar metallicity. The spectrum is only mildly affected by the presence of stripped stars. The largest differences from a population containing only single stars appear at high photon energies ($\gtrsim 40$ eV). This could lead to stronger nebular emission of O III, C IV, and He II than what is expected from single star models.

We present our predictions for properties of stellar populations with metallicities of $Z = 0.006$, 0.002, and 0.0002 in Tables A.1, A.2 and A.3. The general trends of metallicity are discussed in the sections that are mentioned in the tables.

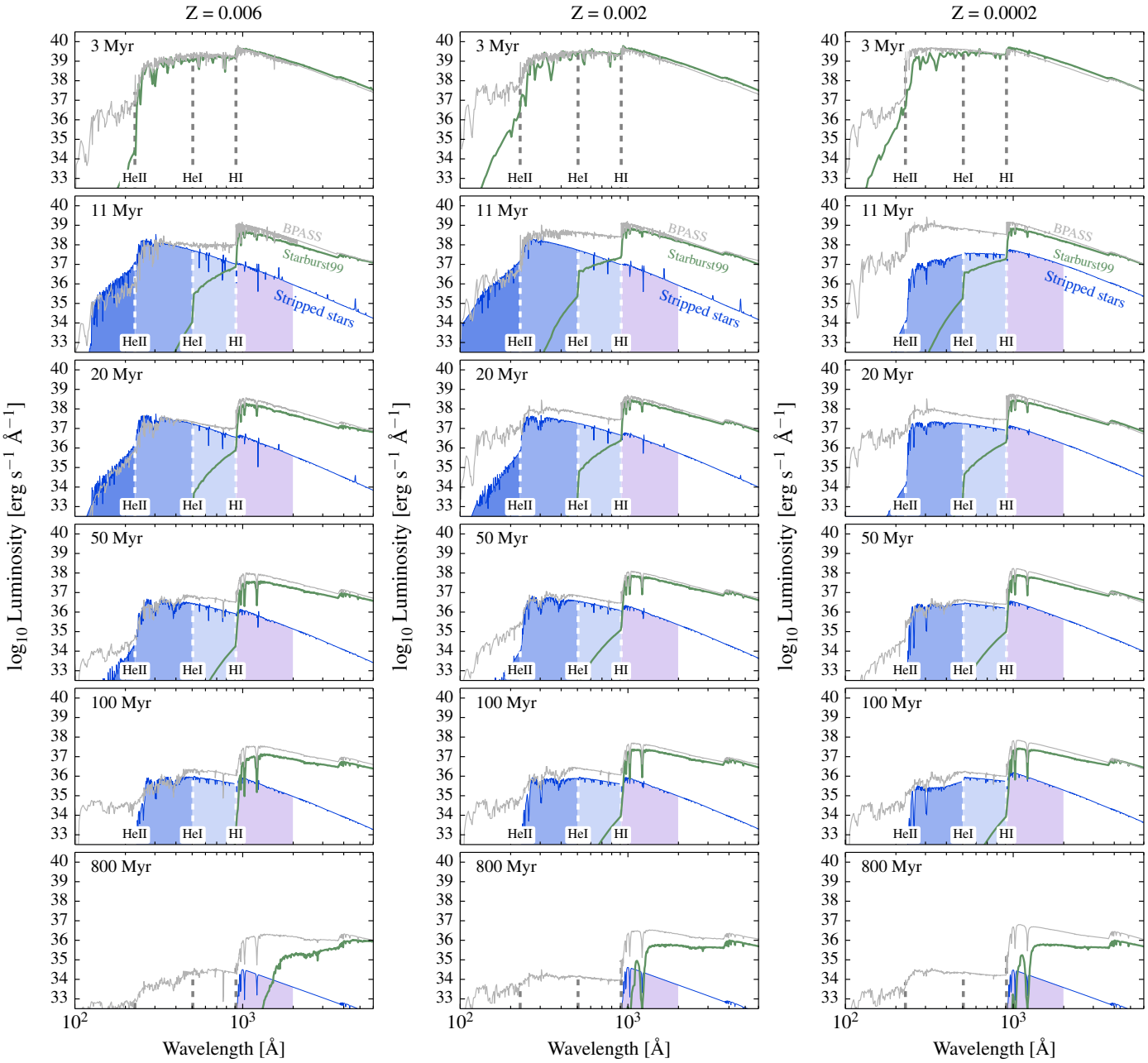

Fig. A.1: The spectral energy distribution of a co-eval stellar population with initially 10^6 $M_\odot$ stars, here shown for metallicities Z = 0.006, 0.002, and 0.0002 (horizontally) and for increasing time after starburst (vertically). The figure is analogous to Fig. 1.

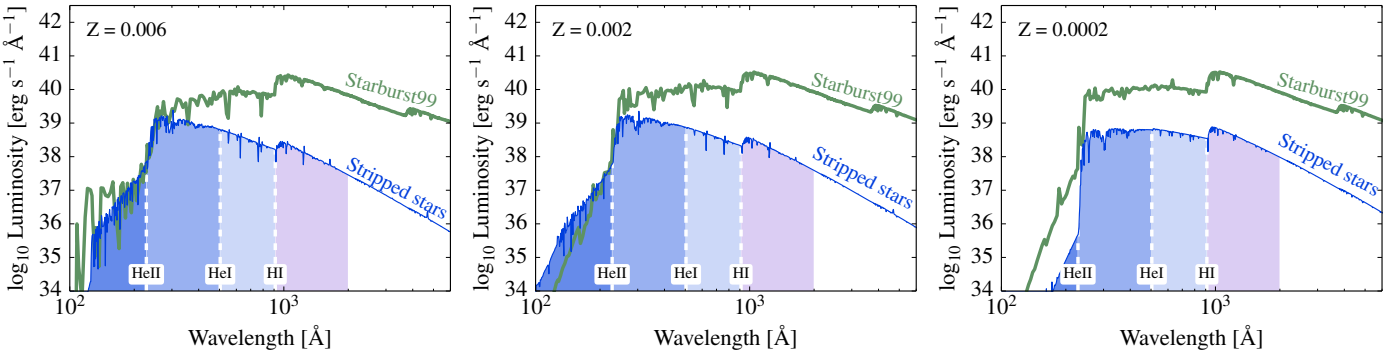

Fig. A.2: The spectral energy distribution in the case of constant star-formation for metallicities Z = 0.006, 0.002, and 0.0002. The models are for 1 $M_\odot$ yr^{-1} and are taken 500 Myr after star-formation started. The figures are analogous to Fig. 2.

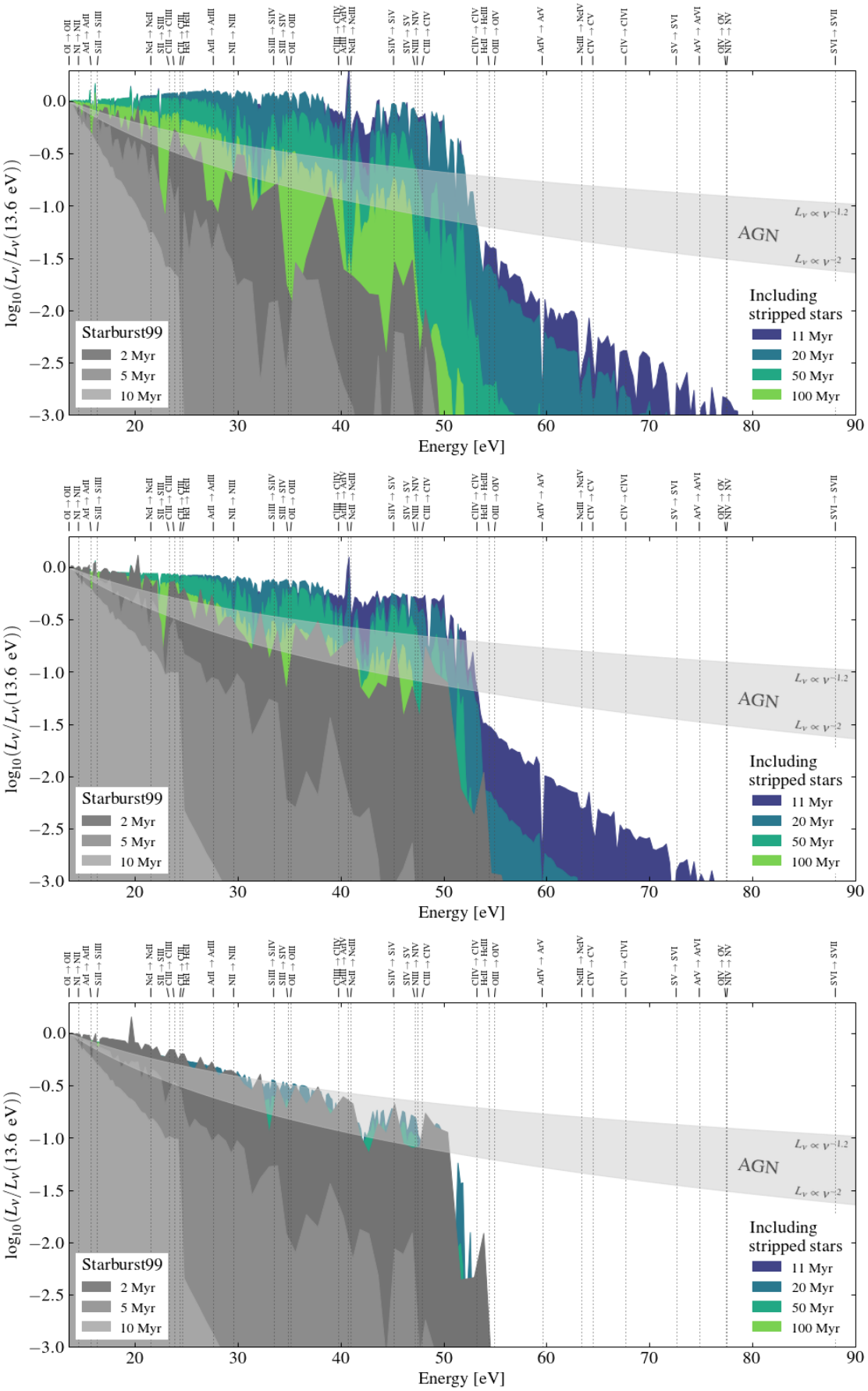

Fig. A.3: The ionizing part of the spectral energy distribution for co-eval stellar populations with metallicities $Z = 0.006$, 0.002, and 0.0002 from top to bottom. The spectra are normalized at the ionization threshold for hydrogen, 13.6 eV. See Fig. 7.

Table A.1: Values of observable quantities for models of stellar populations including stripped stars and at $Z = 0.006$.

Co-eval stellar population ($10^6\ M_\odot$, $Z = 0.006$)									
Time [Myr]	$\log_{10} Q_{0,\mathrm{pop}}$ [s^{-1}]		$\log_{10} Q_{1,\mathrm{pop}}$ [s^{-1}]		$\log_{10} Q_{2,\mathrm{pop}}$ [s^{-1}]		$\log_{10} \xi_{\mathrm{ion},0}$ [$\mathrm{erg}^{-1}\,\mathrm{Hz}$]	$\log_{10} \xi_{\mathrm{ion},1}$ [$\mathrm{erg}^{-1}\,\mathrm{Hz}$]	$\log_{10} \xi_{\mathrm{ion},2}$ [$\mathrm{erg}^{-1}\,\mathrm{Hz}$]	$\log_{10} L_\nu(1500\text{Å})$ [$\mathrm{erg\ s}^{-1}\,\mathrm{Hz}^{-1}$]	$\log_{10} U$	β
Section	4		4		4		5.1.1	5.1.1	5.1.1	5.1.1, 5.2	5.1.2	5.2
2	52.6	(52.6)	51.8	(51.8)	47.5	(47.5)	25.6 (25.6)	24.8 (24.8)	20.5 (20.5)	27.0 (27.0)	−2.0 (−2.0)	−2.95 (−2.95)
3	52.4	(52.4)	51.5	(51.5)	45.5	(45.5)	25.3 (25.3)	24.4 (24.4)	18.4 (18.4)	27.1 (27.1)	−2.1 (−2.1)	−2.58 (−2.58)
5	51.7	(51.7)	50.4	(50.4)	40.3	(40.3)	24.9 (24.9)	23.7 (23.7)	13.5 (13.5)	26.8 (26.8)	−2.3 (−2.3)	−2.54 (−2.54)
7	50.7	(50.7)	47.9	(47.9)	37.5	(37.5)	24.2 (24.2)	21.4 (21.4)	11.0 (11.0)	26.5 (26.5)	−2.6 (−2.6)	−2.52 (−2.52)
11	50.9	(49.7)	50.7	(46.0)	48.4	(−)	24.7 (23.5)	24.5 (19.8)	22.2 (−)	26.2 (26.2)	−2.6 (−3.0)	−2.44 (−2.43)
20	50.4	(48.5)	50.1	(43.4)	47.5	(−)	24.5 (22.7)	24.3 (17.6)	21.7 (−)	25.8 (25.8)	−2.8 (−3.4)	−2.32 (−2.31)
30	50.0	(47.9)	49.6	(41.6)	46.7	(−)	24.3 (22.2)	24.0 (16.0)	21.1 (−)	25.6 (25.6)	−2.9 (−3.6)	−2.1 (−2.09)
50	49.5	(46.8)	49.1	(40.0)	45.6	(−)	24.2 (21.4)	23.8 (14.7)	20.3 (−)	25.3 (25.3)	−3.0 (−4.0)	−1.9 (−1.88)
100	49.1	(45.0)	48.5	(38.1)	43.1	(−)	24.1 (20.0)	23.6 (13.2)	18.2 (−)	24.9 (24.9)	−3.2 (−4.6)	−1.59 (−1.56)
200	48.2	(43.2)	47.1	(−)	40.9	(−)	23.7 (18.7)	22.6 (−)	16.4 (−)	24.5 (24.5)	−3.5 (−5.2)	−1.31 (−1.28)
300	47.5	(41.9)	46.7	(−)	41.6	(−)	23.4 (17.8)	22.5 (−)	17.5 (−)	24.1 (24.1)	−3.7 (−5.6)	−0.58 (−0.49)
500	46.1	(40.1)	43.8	(−)	38.2	(−)	22.6 (16.7)	20.3 (−)	14.8 (−)	23.5 (23.4)	−4.2 (−6.2)	1.3 (1.98)
800	44.8	(37.1)	42.0	(−)	35.9	(−)	22.6 (15.2)	19.8 (−)	13.8 (−)	22.1 (21.8)	−4.6 (−7.2)	4.27 (8.46)
1000	44.2	(36.0)	40.8	(−)	33.7	(−)	22.5 (15.1)	19.1 (−)	12.0 (−)	21.7 (20.9)	−4.8 (−7.5)	4.98 (11.25)
Continuous star-formation ($1\ M_\odot$/year, $Z = 0.006$)												
Time [Myr]	$\log_{10} Q_{0,\mathrm{pop}}$ [s^{-1}]		$\log_{10} Q_{1,\mathrm{pop}}$ [s^{-1}]		$\log_{10} Q_{2,\mathrm{pop}}$ [s^{-1}]		$\log_{10} \xi_{\mathrm{ion},0}$ [$\mathrm{erg}^{-1}\,\mathrm{Hz}$]	$\log_{10} \xi_{\mathrm{ion},1}$ [$\mathrm{erg}^{-1}\,\mathrm{Hz}$]	$\log_{10} \xi_{\mathrm{ion},2}$ [$\mathrm{erg}^{-1}\,\mathrm{Hz}$]	$\log_{10} L_\nu(1500\text{Å})$ [$\mathrm{erg\ s}^{-1}\,\mathrm{Hz}^{-1}$]	$\log_{10} U$	β
Section	4		4		4		5.1.1	5.1.1	5.1.1	5.1.1, 5.2	5.1.2	5.2
500	53.1	(53.1)	52.4	(52.3)	49.4	(49.1)	25.1 (25.1)	24.4 (24.3)	21.4 (21.1)	28.0 (28.0)	−1.8 (−1.9)	−2.34 (−2.34)

Table A.2: Values of observable quantities for models of stellar populations including stripped stars and at $Z = 0.002$.

Co-eval stellar population ($10^6\ M_\odot$, $Z = 0.002$)									
Time [Myr]	$\log_{10} Q_{0,\mathrm{pop}}$ [s^{-1}]	$\log_{10} Q_{1,\mathrm{pop}}$ [s^{-1}]	$\log_{10} Q_{2,\mathrm{pop}}$ [s^{-1}]	$\log_{10} \xi_{\mathrm{ion},0}$ [$\mathrm{erg}^{-1}\,\mathrm{Hz}$]	$\log_{10} \xi_{\mathrm{ion},1}$ [$\mathrm{erg}^{-1}\,\mathrm{Hz}$]	$\log_{10} \xi_{\mathrm{ion},2}$ [$\mathrm{erg}^{-1}\,\mathrm{Hz}$]	$\log_{10} L_\nu(1500\text{Å})$ [$\mathrm{erg\ s}^{-1}\ \mathrm{Hz}^{-1}$]	$\log_{10} U$	β
Section	4	4	4	5.1.1	5.1.1	5.1.1	5.1.1, 5.2	5.1.2	5.2
2	52.7 (52.7)	52.2 (52.2)	48.9 (48.9)	25.8 (25.8)	25.2 (25.2)	21.9 (21.9)	26.9 (26.9)	−2.0 (−2.0)	−3.08 (−3.08)
3	52.6 (52.6)	51.9 (51.9)	47.6 (47.6)	25.5 (25.5)	24.8 (24.8)	20.5 (20.5)	27.1 (27.1)	−2.0 (−2.0)	−2.74 (−2.74)
5	52.0 (52.0)	50.9 (50.9)	45.1 (45.1)	25.2 (25.2)	24.1 (24.1)	18.3 (18.3)	26.8 (26.8)	−2.2 (−2.2)	−2.58 (−2.58)
7	51.4 (51.4)	49.5 (49.5)	39.8 (39.8)	24.7 (24.7)	22.9 (22.9)	13.1 (13.1)	26.7 (26.7)	−2.4 (−2.4)	−2.51 (−2.51)
11	51.0 (50.3)	50.7 (47.4)	48.6 (37.1)	24.7 (23.9)	24.4 (21.0)	22.2 (10.7)	26.4 (26.4)	−2.5 (−2.8)	−2.43 (−2.42)
20	50.4 (49.1)	50.1 (45.2)	47.1 (−)	24.4 (23.2)	24.1 (19.2)	21.1 (−)	26.0 (26.0)	−2.7 (−3.2)	−2.34 (−2.33)
30	50.1 (48.5)	49.8 (43.8)	46.4 (−)	24.3 (22.7)	24.0 (18.0)	20.6 (−)	25.8 (25.8)	−2.9 (−3.4)	−2.28 (−2.27)
50	49.7 (47.7)	49.3 (41.8)	45.2 (−)	24.1 (22.2)	23.7 (16.3)	19.7 (−)	25.5 (25.5)	−3.0 (−3.7)	−2.1 (−2.09)
100	49.0 (46.5)	48.5 (40.1)	43.0 (−)	23.9 (21.3)	23.3 (15.0)	17.9 (−)	25.1 (25.1)	−3.2 (−4.1)	−1.84 (−1.82)
200	48.3 (44.9)	47.2 (38.4)	41.6 (−)	23.6 (20.2)	22.5 (13.6)	16.9 (−)	24.7 (24.7)	−3.5 (−4.6)	−1.54 (−1.52)
300	47.6 (43.9)	46.8 (36.4)	41.8 (−)	23.2 (19.5)	22.4 (12.0)	17.4 (−)	24.5 (24.5)	−3.7 (−4.9)	−1.33 (−1.3)
500	46.2 (42.9)	44.6 (−)	39.9 (−)	22.1 (18.8)	20.5 (−)	15.8 (−)	24.1 (24.1)	−4.1 (−5.3)	−0.97 (−0.93)
800	45.0 (41.5)	42.1 (−)	36.0 (−)	21.3 (17.9)	18.5 (−)	12.4 (−)	23.6 (23.6)	−4.6 (−5.7)	0.09 (0.19)
1000	44.3 (40.8)	41.2 (−)	34.2 (−)	20.9 (17.5)	17.8 (−)	10.8 (−)	23.4 (23.4)	−4.8 (−5.9)	0.97 (1.11)
Continuous star-formation (1 $M_\odot$/year, $Z = 0.002$)									
Time [Myr]	$\log_{10} Q_{0,\mathrm{pop}}$ [s^{-1}]	$\log_{10} Q_{1,\mathrm{pop}}$ [s^{-1}]	$\log_{10} Q_{2,\mathrm{pop}}$ [s^{-1}]	$\log_{10} \xi_{\mathrm{ion},0}$ [$\mathrm{erg}^{-1}\,\mathrm{Hz}$]	$\log_{10} \xi_{\mathrm{ion},1}$ [$\mathrm{erg}^{-1}\,\mathrm{Hz}$]	$\log_{10} \xi_{\mathrm{ion},2}$ [$\mathrm{erg}^{-1}\,\mathrm{Hz}$]	$\log_{10} L_\nu(1500\text{Å})$ [$\mathrm{erg\ s}^{-1}\ \mathrm{Hz}^{-1}$]	$\log_{10} U$	β
Section	4	4	4	5.1.1	5.1.1	5.1.1	5.1.1, 5.2	5.1.2	5.2
500	53.3 (53.3)	52.6 (52.6)	49.4 (49.1)	25.2 (25.2)	24.6 (24.5)	21.3 (21.0)	28.1 (28.1)	−1.8 (−1.8)	−2.35 (−2.35)

Table A.3: Values of observable quantities for models of stellar populations including stripped stars and at $Z = 0.0002$.

Co-eval stellar population ($10^6\ M_\odot$, $Z = 0.0002$)									
Time [Myr] Section	$\log_{10} Q_{0,\mathrm{pop}}$ [s^{-1}] 4		$\log_{10} Q_{1,\mathrm{pop}}$ [s^{-1}] 4		$\log_{10} Q_{2,\mathrm{pop}}$ [s^{-1}] 4		$\log_{10} \xi_{\mathrm{ion},0}$ [$\mathrm{erg}^{-1}\,\mathrm{Hz}$] 5.1.1		$\log_{10} \xi_{\mathrm{ion},1}$ [$\mathrm{erg}^{-1}\,\mathrm{Hz}$] 5.1.1		$\log_{10} \xi_{\mathrm{ion},2}$ [$\mathrm{erg}^{-1}\,\mathrm{Hz}$] 5.1.1		$\log_{10} L_\nu(1500\text{Å})$ [$\mathrm{erg\ s^{-1}\ Hz^{-1}}$] 5.1.1, 5.2		$\log_{10} U$ 5.1.2		β 5.2	
2	52.8	(52.8)	52.2	(52.2)	48.6	(48.6)	25.9	(25.9)	25.3	(25.3)	21.7	(21.7)	26.9	(26.9)	−2.0	(−2.0)	−3.08	(−3.08)
3	52.6	(52.6)	52.0	(52.0)	47.8	(47.8)	25.5	(25.5)	24.8	(24.8)	20.7	(20.7)	27.1	(27.1)	−2.0	(−2.0)	−2.77	(−2.77)
5	52.0	(52.0)	50.9	(50.9)	45.8	(45.8)	25.2	(25.2)	24.1	(24.1)	19.0	(19.0)	26.8	(26.8)	−2.2	(−2.2)	−2.61	(−2.61)
7	51.4	(51.4)	49.6	(49.6)	40.1	(40.1)	24.7	(24.7)	23.0	(23.0)	13.4	(13.4)	26.7	(26.7)	−2.4	(−2.4)	−2.57	(−2.57)
11	50.9	(50.2)	50.0	(47.3)	45.2	(37.2)	24.5	(23.8)	23.6	(20.9)	18.8	(10.8)	26.4	(26.4)	−2.6	(−2.8)	−2.52	(−2.5)
20	50.4	(49.0)	49.9	(45.1)	45.3	(−)	24.4	(23.0)	23.9	(19.1)	19.3	(−)	26.0	(26.0)	−2.7	(−3.2)	−2.41	(−2.39)
30	50.1	(48.4)	49.6	(43.9)	44.9	(−)	24.3	(22.6)	23.8	(18.1)	19.1	(−)	25.8	(25.8)	−2.8	(−3.4)	−2.34	(−2.32)
50	49.6	(47.6)	49.0	(42.1)	44.0	(−)	24.1	(22.1)	23.5	(16.6)	18.4	(−)	25.5	(25.5)	−3.0	(−3.7)	−2.15	(−2.13)
100	49.0	(46.4)	48.2	(40.5)	42.8	(−)	23.9	(21.3)	23.0	(15.3)	17.7	(−)	25.1	(25.1)	−3.2	(−4.1)	−1.88	(−1.85)
200	48.2	(45.1)	46.8	(38.8)	41.3	(−)	23.5	(20.4)	22.1	(14.1)	16.6	(−)	24.7	(24.7)	−3.5	(−4.5)	−1.57	(−1.53)
300	47.1	(44.3)	45.3	(37.0)	40.1	(−)	22.7	(19.8)	20.9	(12.6)	15.7	(−)	24.5	(24.5)	−3.8	(−4.8)	−1.34	(−1.3)
500	46.2	(43.3)	44.9	(−)	40.3	(−)	22.1	(19.2)	20.8	(−)	16.2	(−)	24.1	(24.1)	−4.1	(−5.1)	−0.96	(−0.91)
800	44.7	(42.0)	41.8	(−)	35.5	(−)	21.1	(18.3)	18.2	(−)	11.8	(−)	23.7	(23.6)	−4.6	(−5.6)	0.07	(0.14)
1000	41.4	(41.4)	–	(−)	–	(−)	18.0	(18.0)	–	(−)	–	(−)	23.4	(23.4)	−5.8	(−5.8)	1.03	(1.03)
Continuous star-formation ($1\ M_\odot$/year, $Z = 0.0002$)																		
Time [Myr] Section	$\log_{10} Q_{0,\mathrm{pop}}$ [s^{-1}] 4		$\log_{10} Q_{1,\mathrm{pop}}$ [s^{-1}] 4		$\log_{10} Q_{2,\mathrm{pop}}$ [s^{-1}] 4		$\log_{10} \xi_{\mathrm{ion},0}$ [$\mathrm{erg}^{-1}\,\mathrm{Hz}$] 5.1.1		$\log_{10} \xi_{\mathrm{ion},1}$ [$\mathrm{erg}^{-1}\,\mathrm{Hz}$] 5.1.1		$\log_{10} \xi_{\mathrm{ion},2}$ [$\mathrm{erg}^{-1}\,\mathrm{Hz}$] 5.1.1		$\log_{10} L_\nu(1500\text{Å})$ [$\mathrm{erg\ s^{-1}\ Hz^{-1}}$] 5.1.1, 5.2		$\log_{10} U$ 5.1.2		β 5.2	
500	53.3	(53.3)	52.7	(52.6)	48.9	(48.9)	25.2	(25.2)	24.6	(24.6)	20.8	(20.8)	28.1	(28.1)	−1.8	(−1.8)	−2.39	(−2.38)

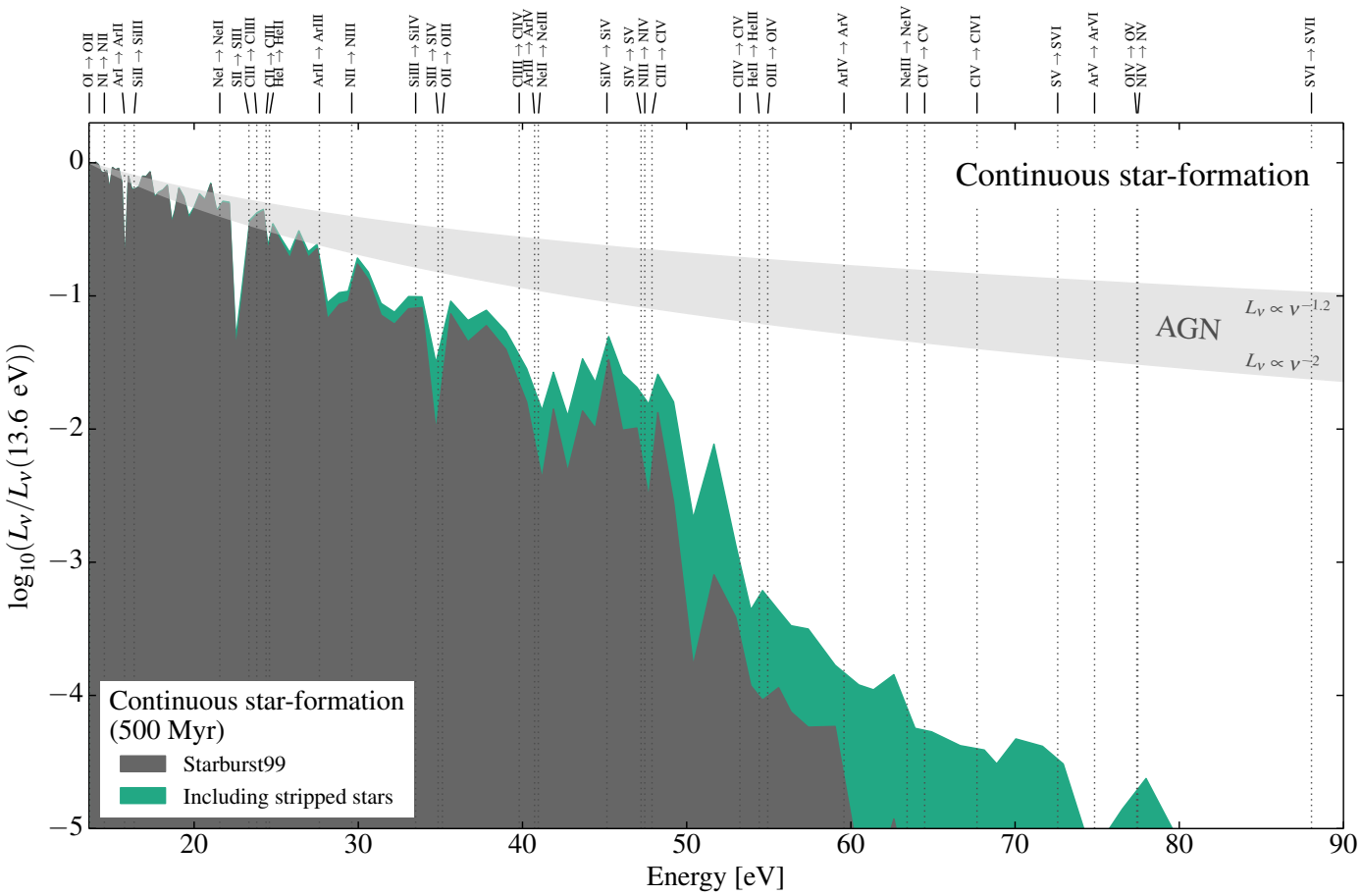

Fig. A.4: The ionizing part of the spectral energy distribution in the case of continuous star-formation, taken after 500 Myr. We compare a population containing only single stars (gray) with one containing also stripped stars (green). We show models for solar metallicity. See also Fig. 7.